Inorg. Chem. **2006**, *45*, 4830–4844

Inorganic Chemistry
Article

Synthesis, Reactivities, and Magnetostructural Properties of Fe^{III}, Fe^{III}–O–Fe^{III}, and $Zn^{II}Fe^{III}$–O–$Fe^{III}Zn^{II}$ Complexes of a Tetraiminodiphenolate Macrocycle

Papu Biswas,[†] Meenakshi Ghosh,[†] Sujit K. Dutta,[†] Ulrich Flörke,[‡] and Kamalaksha Nag*,[†]

Department of Inorganic Chemistry, Indian Association for the Cultivation of Science, Jadavpur,
Kolkata 700032, India, and Anorganische und Analytische Chemie, Universität Paderborn,
D-33098 Paderborn, Germany

Received February 1, 2006

The mononuclear iron(III) complexes $[Fe(LH_2)(H_2O)Cl](ClO_4)_2{\cdot}2H_2O$ (**1**) and $[Fe(LH_2)(H_2O)_2](ClO_4)_3{\cdot}H_2O$ (**2**) have been prepared by reacting $[Pb(LH_2)](ClO_4)_2$ with $FeCl_3{\cdot}6H_2O$ and $Fe(ClO_4)_3{\cdot}6H_2O$, respectively. Complex **2** upon treatment with 1 equiv of alkali produces the oxo-bridged dimer $[\{Fe(LH_2)(H_2O)\}_2(\mu\text{-}O)](ClO_4)_4{\cdot}2H_2O$ (**3**). In these compounds, LH_2 refers to the tetraiminodiphenol macrocycle in the zwitterionic form whose two uncoordinated imine nitrogens are protonated and hydrogen-bonded to the metal-bound phenolate oxygens. The aqua ligands of complexes **1**–**3** get exchanged in acetonitrile. Reaction equilibria involving binding and exchange of the terminal ligands ($Cl^-/H_2O/CH_3CN$) in these complexes have been studied spectrophotometrically. The equilibrium constant for the aquation reaction (K_{aq}) $[\mathbf{1}]^{2+} + H_2O \overset{K_{aq}}{\rightleftharpoons} [\mathbf{2}]^{3+} + Cl^-$ in acetonitrile is 8.65(5) M, and the binding constant (K_{Cl^-}) for the reaction $[\mathbf{1}]^{2+} + Cl^- \overset{K_{Cl^-}}{\rightleftharpoons} [\mathbf{1}Cl]^+ + CH_3CN$ is 4.75(5) M. The pK_D value for the dimerization reaction $2[\mathbf{2}]^{3+} + 2OH^- \overset{K_D}{\rightleftharpoons} [\mathbf{3}]^{4+} + 3H_2O$ in 1:1 acetonitrile–water is 9.38(10). Complexes **1**–**3** upon reaction with $Zn(ClO_4)_2{\cdot}6H_2O$ and sodium acetate (OAc), pivalate (OPiv), or bis(4-nitrophenyl)phosphate (BNPP) produce the heterobimetallic complexes $[\{FeLZn(\mu\text{-}X)\}_2(\mu\text{-}O)](ClO_4)_2$, where X = OAc (**4**), OPiv (**5**), and BNPP (**6**). The pseudo-first-order rate constant (k_{obs}) for the formation of **4** at 25 °C from either **1** or **3** with an excess of $Zn(OAc)_2{\cdot}2H_2O$ in 1:1 acetonitrile–water at pH 6.6 is found to be the same with $k_{obs} = 1.6(2) \times 10^{-4}\ s^{-1}$. The X-ray crystal structures of **3**, **4**, and **6** have been determined, although the structure determination of **3** was severely affected because of heavy disordering. In **3**, the Fe–O–Fe angle is 168.6(6)°, while it is exactly 180.0° in **4** and **6**. Cyclic and square-wave voltammetric (CV and SWV) measurements have been carried out for complexes **1**–**4** in acetonitrile. The variation of the solvent composition (acetonitrile–water) has a profound effect on the $E_{1/2}$ and ΔE_p values. The binding of an additional chloride ion to an iron(III) center in **1**–**3** is accompanied by a remarkable shift of $E_{1/2}$ to more negative values. The observation of quasi-reversible CV for complexes containing a Fe^{III}–O–Fe^{III} unit (**3** and **4**) indicates that in the electrochemical time scale unusual Fe^{III}–O–Fe^{II} is produced. The ^1H NMR spectra of complexes **3**–**6** exhibit hyperfine-shifted signals in the range 0–90 ppm with similar features. The metal–hydrogen distances obtained from T_1 measurements are in good agreement with the crystallographic data. Variable-temperature (2–300 K) magnetic susceptibility measurements carried out for **3** and **4** indicate strong antiferromagnetic exchange interaction ($H = -2JS_1{\cdot}S_2$) between the high-spin iron(III) centers in the Fe–O–Fe unit with $J = -114\ cm^{-1}$ (**3**) and $-107\ cm^{-1}$ (**4**).

Introduction

The question of whether dimerization of $[Fe(H_2O)_6]^{3+}$ occurs through the formation of the oxo-bridged $[(H_2O)_5Fe(\mu\text{-}O)Fe(H_2O)_5]^{4+}$ or the dihydroxy-bridged $[(H_2O)_4Fe(\mu\text{-}OH)_2Fe(H_2O)_4]^{4+}$ species is a still debated issue.[1] Nevertheless, the perchlorate and nitrate salts of the oxo-bridged aqua ion $[(H_2O)_5Fe(\mu\text{-}O)Fe(H_2O)_5]^{4+}$ have recently been isolated

---

* To whom correspondence should be addressed: E-mail: ickn@mahendra.iacs.res.in.

[†] Indian Association for the Cultivation of Science.

[‡] Universität Paderborn.

(1) Lente, G.; Fabian, I. *Inorg. Chem.* **1999**, *38*, 603 and references cited therein.

10.1021/ic060183b CCC: $33.50

as the crown ether adducts, and their crystal structures have been determined.[2]

The occurrences of μ-O and μ-$(OH)_2$ diiron(III) species have major implications in the reactivity of non-heme iron proteins. Hemerythrin (a dioxygen carrier) and ribonucleotide reductase (a tyrosyl radical generator) in their oxidized resting states contain an oxo- and carboxylate-bridged diiron(III) unit, whereas methane monooxygenase (a catalyst for the conversion of methane to methanol) in its oxidized resting state contains a dihydroxy- and carboxylate-bridged diiron(III) unit. Consequently, over the past 2 decades, extensive studies have been made on diiron complexes as structural and functional models of non-heme diiron proteins.[3−7] Aside from the diiron proteins, purple acid phosphatases are another type of iron(III)-containing dinuclear metalloenzyme, which catalyzes the hydrolysis of phosphate esters at pH 4−7. Purple acid phosphatase isolated from plant sources such as red kidney bean contains the $Fe^{III}Zn^{II}$ unit, and that isolated from sweet potato contains the $Fe^{III}Mn^{II}$ unit,[8] while those isolated from mammalian sources (such as bovine spleen, porcine uterus fluid, etc.) contain the $Fe^{III}Fe^{II}$ unit. Despite the difference in metal contents, the enzymetic activities of purple acid phosphatases obtained from different sources, however, are similar.[9−11] The crystal structure of the enzymatically active kidney bean purple acid phosphatase (KBPAP) has been determined,[12] and the active site of the six-coordinated iron(III) and zinc(II) centers has been modeled with three exogenous H_2O/OH^- ligands, of which a terminal OH^- is bound to iron(III), a terminal H_2O is ligated to zinc(II), and another OH^- ligand along with a carboxylate oxygen bridge the two metal centers. The iron(III) is further coordinated by each of a phenol, imidazole, and carboxylate residue, while the zinc(II) is coordinated by two imidazole residues and an amide unit. Crystal structures of purple acid phosphatases in phosphate-ligated form obtained from other sources have been reported.[13−17] Several heterodinuclear Fe^{III}-Zn^{II} and mixed-valence $Fe^{III}Fe^{II}$ complexes have been reported[18−31] as structural/functional models of purple acid phosphatases.

We have earlier reported carboxylate-bridged dinuclear zinc(II)[32] and valence-delocalized iron(II)−iron(III)[33] complexes of the tetraiminodiphenol macrocyclic ligand H_2L. In the present study, the chemistry of Fe−O−Fe-linked carboxylate- and phosphate-bridged heterobimetallic iron(III)−zinc(II) complexes has been reported. In view of the important roles played by exogenous terminal ligands in non-heme iron proteins, the reaction equilibria involving binding and exchange of the terminal ligands ($H_2O/CH_3CN/Cl^-$) in the mononuclear iron(III) and oxo-bridged diiron(III) complexes have been studied in detail.

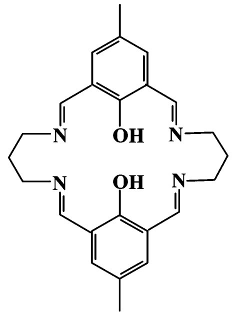

H_2L

Experimental Section

Materials. Reagent-grade chemicals obtained from commercial sources were used as received. Solvents were purified and dried according to standard methods.[34] The buffer solutions were prepared with [2-(*N*-morpholino)ethanesulfonic acid], [tris(hydroxymethyl)-

---

(2) (a) Junk, P. C.; McCool, B. J.; Moubaraki, B.; Murray, K. S.; Spiccia, L. *Angew. Chem., Int. Ed.* **1999**, *38*, 2224. (b) Junk, P. C.; McCool, B. J.; Moubaraki, B.; Murray, K. S.; Spiccia, L.; Cashion, J. D.; Steed, J. W. *J. Chem. Soc., Dalton Trans.* **2002**, 1024.

(3) Kurtz, D. M., Jr. *Chem. Rev.* **1990**, *90*, 585.

(4) (a) Que, L., Jr. *J. Chem. Soc., Dalton Trans.* **1997**, 3933. (b) Que, L., Jr.; Tolman, W. B. *Angew. Chem., Int. Ed.* **2002**, *41*, 1114.

(5) Fontecave, M.; Ménage, S.; Duboc-Toia, C. *Coord. Chem. Rev.* **1998**, *178−180*, 1555.

(6) Bois, J. Du.; Mizoguchi, T. J.; Lippard, S. J. *Coord. Chem. Rev.* **2000**, *200−202*, 443.

(7) Tshuva, E. Y.; Lippard, S. J. *Coord. Chem. Rev.* **2004**, *104*, 987.

(8) Schenk, G.; Boutchard, C. L.; Carrington, L. E.; Nobles, C. J.; Moubaraki, B.; Murray, K. S.; de Jessey, J.; Hanson, G. R. *J. Biol. Chem.* **2001**, *276*, 19084.

(9) Wilcox, D. E. *Chem. Rev.* **1996**, *96*, 2435.

(10) Klabunde, T.; Krebs, B. *Struct. Bonding* **1997**, *89*, 177.

(11) Twichett, M. B.; Sykes, A. G. *Eur. J. Inorg. Chem.* **1999**, 2105.

(12) Sträter, N.; Klabunde, T.; Tucker, P.; Witzel, H.; Krebs, B. *Science* **1996**, *268*, 1489.

(13) Klabunde, T.; Sträter, N.; Fröhlich, R.; Witzel, H.; Krebs, B. *J. Mol. Biol.* **1996**, *259*, 737.

(14) Guddat, I. W.; McAlpine, A. S.; Hume, D.; Hamilton, S. *Structure* **1999**, *7*, 757.

(15) Lindquist, Y.; Johansson, I.; Kaija, H.; Vhiko, P.; Schneider, G. *J. Mol. Biol.* **1999**, *291*, 135.

(16) Uppenberg, J.; Lindquist, I.; Svensson, C.; Ek-Rylander, B.; Andersson, G. *J. Mol. Biol.* **1999**, *290*, 201.

(17) Schenk, G.; Gahan, L. R.; Carrington, L. E.; Mitic, N.; Valizadeh, M.; Guddat, L. W. *Proc. Natl. Acad. Sci.* **2005**, *102*, 273.

(18) Belle, C.; Gautier-Luneau, I.; Karmazin, L.; Pierre, J.-L.; Albedyhl, S. *Eur. J. Inorg. Chem.* **2002**, 3087.

(19) Albedyhl, S.; Schneiders, D.; Jansćo, A.; Gajda, T.; Krebs, B. *Eur. J. Inorg. Chem.* **2002**, 1400.

(20) Albedyhl, S.; Averbuch-Pouchot, M. T.; Belle, C.; Krebs, B.; Pierre, J. L.; Saint-Aman, E.; Torelli, S. *Eur. J. Inorg. Chem.* **2001**, 1457.

(21) Neves, A.; Rossi, L. M.; Vencato, I.; Hasse, W.; Werner, R. *J. Chem. Soc., Dalton Trans.* **2000**, 707.

(22) Than, R.; Feldmann, A. A.; Krebs, B. *Coord. Chem. Rev.* **1999**, *182*, 211.

(23) Kamitani, J.; Kawahara, R.; Yashiro, N.; Komiyama, M. *Chem. Lett.* **1998**, 1047.

(24) Ghiladi, M.; McKenzie, C. J.; Meier, A.; Powell, A. K.; Ulstrup, J.; Wocadlo, S. *J. Chem. Soc., Dalton Trans.* **1997**, 4011.

(25) Lambert, E.; Chabut, B.; Chardon-Noblat, S.; Deronzier, A.; Chottard, G.; Bousseksou, A.; Tuchagues, J. P.; Laugier, J.; Bardet, M.; Latour, J. M. *J. Am. Chem. Soc.* **1997**, *119*, 9424.

(26) Yin, L.; Cheng, P.; Yao, X.; Wang, H. *J. Chem. Soc., Dalton Trans.* **1997**, 2109.

(27) Duboc-Toia, C.; Ménage, S.; Vincent, J. M.; Averbuch-Pouchot, M. T.; Fontecave, M. *Inorg. Chem.* **1997**, *36*, 6148.

(28) Dutta, S. K.; Werner, R.; Flörke, U.; Mohanta, S.; Nanda, K. K.; Hasse, W.; Nag, K. *Inorg. Chem.* **1996**, *35*, 2292.

(29) Bernard, E.; Monata, W.; Laugier, J.; Chardon-Nobalt, S.; Deronzier, A.; Tuchagues, J. P.; Latour, J. M. *Angew. Chem., Int. Ed. Engl.* **1994**, *33*, 887.

(30) Krebs, B.; Schepers, K.; Bremer, B.; Henkel, G.; Althaus, E.; Müller-Warmuth, W.; Griesar, K.; Hasse, W. *Inorg. Chem.* **1994**, *33*, 1907.

(31) Schepers, K.; Bremer, B.; Krebs, B.; Henkel, G.; Althaus, E.; Müller-Warmuth, W.; Griesar, K.; Hasse, W. *Angew. Chem., Int. Ed. Engl.* **1990**, *29*, 531.

(32) Dutta, B.; Bag, P.; Flörke, U.; Nag, K. *Inorg. Chem.* **2005**, *44*, 147.

(33) Dutta, S. K.; Ensling, J.; Werner, R.; Flörke, U.; Hasse, W.; Gütlich, P.; Nag, K. *Angew. Chem., Int. Ed. Engl.* **1997**, *36*, 152.

(34) Perrin, D. D.; Armarego, W. L.; Perrin, D. R. *Purification of Laboratory Chemicals*, 2nd ed.; Pergamon: Oxford, U.K., 1980.

aminomethane], or sodium acetate as reported in the literature.[35] 2,6-Diformyl-4-methylphenol was prepared according to the literature method,[36] while $[H_2LH_2](ClO_4)_2$[37] and $[Pb(LH_2)](ClO_4)_2$[38] were prepared as reported earlier by us. Bis(4-nitrophenyl)phosphate (BNPP) was prepared according to a reported procedure.[39]

Caution! *The perchlorate salts reported in this study are potentially explosive and therefore should be handled in small amounts with care.*

Preparation of the Complexes. $[Fe(LH_2)(H_2O)Cl](ClO_4)_2\cdot 2H_2O$ (1). To a stirred suspension of $[Pb(LH_2)](ClO_4)_2$ (0.81 g, 1 mmol) in methanol (50 mL) was added a methanol solution (10 mL) of $FeCl_3\cdot 6H_2O$ (0.27 g, 1 mmol). After 1 h of stirring, the precipitated $PbCl_2$ was filtered off. The filtrate was concentrated to ca. 30 mL on a rotary evaporator, and 0.5 g of $NaClO_4$ was added to it. The solution was kept at room temperature for an overnight period, during which time shiny deep-red-violet crystals deposited. The product was filtered and recrystallized from methanol. Yield: 0.61 g (81%). Anal. Calcd for $C_{24}H_{34}Cl_3FeN_4O_{13}$: C, 38.50; H, 4.58; N, 7.48. Found: C, 38.36; H, 4.62; N, 7.56. FT-IR (KBr, ν/cm^{-1}): 3420(br), 3165(w), 1657(s), 1626(s), 1557(s), 1447(m), 1350(m), 1281(m), 1238(m), 1087(s, br), 873(w), 818(w), 628(m), 514(w). UV−vis [CH_3CN, λ_{max}/nm (ϵ/M^{-1} cm^{-1})]: 385 (13 800), 435(sh), 530 (3600). Λ_M (CH_3CN/Ω^{-1} cm^2 M^{-1}): 290.

$[Fe(LH_2)(H_2O)_2](ClO_4)_3\cdot H_2O$ (2). This compound can be prepared in the same way as **1** by using $Fe(ClO_4)_3\cdot 6H_2O$. Alternatively, it can be prepared in the following way: To an acetonitrile solution (30 mL) of the perchlorate salt of the macrocyclic ligand $[H_2LH_2](ClO_4)_2$ (0.61 g, 1 mmol) was added $Fe(ClO_4)_3\cdot 6H_2O$ (0.46 g, 1 mmol) in portions. The solution was stirred for 0.5 h and then concentrated on a rotary evaporator to ca. 10 mL. To this was added with stirring a methanol solution (10 mL) of $NaClO_4$ (0.5 g). A deep-red crystalline product that deposited was collected by filtration and washed with ethanol and diethyl ether. Yield: 0.61 g (75%). Anal. Calcd for $C_{24}H_{34}Cl_3FeN_4O_{17}$: C, 35.47; H, 4.22; N, 6.89. Found: C, 35.29; H, 4.29; N, 6.98. FT-IR (KBr, ν/cm^{-1}): 3430(br), 3175(w), 1660(s), 1624(m), 1556(s), 1446(m), 1348(m), 1282(m), 1238(m), 1100(s, br), 866(w), 818(w), 629(m), 517(w). UV−vis [CH_3CN, λ_{max}/nm (ϵ/M^{-1} cm^{-1})]: 375 (13 500), 555 (3200). Λ_M (CH_3CN/Ω^{-1} cm^2 M^{-1}): 365.

$[\{Fe(LH_2)(H_2O)\}_2(\mu\text{-}O)](ClO_4)_4\cdot 2H_2O$ (3). To a stirred acetonitrile−ethanol (1:1) solution (50 mL) of **1** (0.75 g, 1 mmol) was added solid $AgClO_4$ (0.21 g, 1 mmol). AgCl that precipitated was removed by filtration. The filtrate was slowly treated with 1 mL of aqueous sodium hydroxide (1 M), when the solution changed from dark violet to deep red. Upon concentration of the solution at 80 °C to ca. 20 mL, a red crystalline product began to deposit. After the solution was left standing at room temperature for 2 h, the product was filtered off and recrystallized from acetonitrile−ethanol (1:2). Yield: 0.59 g (84%). ESI-MS (CH_3CN): 1234.9 (2%) $[\{Fe_2(LH_2)(H_2O)(\mu\text{-}O)(ClO_4)_3]^+$; 1134.5 (3%) $[\{Fe_2(LH_2)(LH)(\mu\text{-}O)(ClO_4)_2]^+$; 1034.1 (8%) $[\{Fe_2(LH)_2(\mu\text{-}O)(ClO_4)]^+$; 558.1 (70%) $[Fe(LH)(ClO_4)]^+$. Anal. Calcd for $C_{48}H_{64}Cl_4Fe_2N_8O_{25}$: C, 40.99; H, 4.59; N, 7.97. Found: C, 41.22; H, 4.52; N, 7.91. FT-IR (KBr, ν/cm^{-1}): 3440(br), 3160(w), 1652(s), 1631(sh), 1552(s), 1449(m), 1352(m), 1280(w), 1238(m), 1090(s), 854(m), 818(m), 673(w), 625(m), 513(w). UV−vis [CH_3CN, λ_{max}/nm (ϵ/M^{-1} cm^{-1})]: 392 (29 000), 425(sh). Λ_M (CH_3NO_2/Ω^{-1} cm^2 M^{-1}): 300.

$[\{FeLZn(\mu\text{-}OAc)\}_2(\mu\text{-}O)](ClO_4)_2\cdot H_2O$ (4). An acetonitrile solution (30 mL) of **1** (0.75 g, 1 mmol) was treated with $Zn(ClO_4)_2\cdot 6H_2O$ (0.37 g, 1 mmol) followed by the addition of 20 mL of an ethanol solution of sodium acetate (0.66 g, 8 mmol). A red crystalline product that deposited over a period of 6 h was collected by filtration and recrystallized from methanol−acetonitrile (1:1). Yield: 0.59 g (84%). ESI-MS (CH_3CN): 1280.6 (6%) $[\{FeLZn(\mu\text{-}OAc)\}_2(\mu\text{-}O)(ClO_4)]^+$; 590.2 (100%) $[\{FeLZn(\mu\text{-}OAc)\}_2(\mu\text{-}O)]^{2+}$. Anal. Calcd for $C_{52}H_{60}Cl_2Fe_2N_8O_{18}Zn_2$: C, 44.66; H, 4.32; N, 8.01. Found: C, 44.80; H, 4.37; N, 8.08. FT-IR (KBr, ν/cm^{-1}): 3400(br), 1633(s), 1606(sh), 1564(s), 1440(m), 1408(m), 1326(m), 1278(w), 1241(w), 1199(w), 1090(s), 847(m), 819(m), 767(w), 668(w), 628(m), 523(w). UV−vis [CH_3CN, λ_{max}/nm (ϵ/M^{-1} cm^{-1})]: 360 (25 000). Λ_M (CH_3CN/Ω^{-1} cm^2 M^{-1}): 280.

$[\{FeLZn(\mu\text{-}OPiv)\}_2(\mu\text{-}O)](ClO_4)_2\cdot H_2O$ (5). To an acetonitrile solution (25 mL) of **2** (0.35 g, 0.25 mmol) was added an ethanol solution (25 mL) containing $Zn(ClO_4)_2\cdot 6H_2O$ (0.19 g, 0.5 mmol) and sodium pivalate (0.5 g, 4 mmol). The solution was kept at room temperature to undergo slow evaporation. The red microcrystalline product that deposited was filtered and recrystallized from methanol−acetonitrile (1:1). Yield: 0.28 g (77%). ESI-MS (CH_3CN): 1364.2 (4%) $[\{FeLZn(\mu\text{-}OPiv)\}_2(\mu\text{-}O)(ClO_4)]^+$; 632.4 (15%) $[\{FeLZn(\mu\text{-}OPiv)\}_2(\mu\text{-}O)]^{2+}$. Anal. Calcd for $C_{58}H_{72}Cl_2Fe_2N_8O_{18}Zn_2$: C, 46.99; H, 4.89; N, 7.56. Found: C, 46.81; H, 4.98; N, 7.61. FT-IR (KBr, ν/cm^{-1}): 3420(br), 1637(s), 1608(m), 1562(s), 1443(m), 1408(m), 1325(m), 1277(w), 1236(w), 1100(s,br), 848(m), 816(m), 768(w), 629(m), 525(w). UV−vis [CH_3CN, λ_{max}/nm (ϵ/M^{-1} cm^{-1})]: 363 (25 600). Λ_M (CH_3CN/Ω^{-1} cm^2 M^{-1}): 270.

$[\{FeLZn(\mu\text{-}BNPP)\}_2(\mu\text{-}O)](ClO_4)_2$ (6). To an acetonitrile solution (30 mL) of **1** (0.38 g, 0.5 mmol) were added solid $Zn(ClO_4)_2\cdot 6H_2O$ (0.19 g, 0.5 mmol) and a methanol solution (10 mL) of BNPP (0.34 g, 1 mmol) and triethylamine (0.1 g, 1 mmol). The solution was kept for an overnight period, during which time a red crystalline product deposited. This was filtered and recrystallized from methanol−acetonitrile (1:1). Yield: 0.45 g (92%). ESI-MS (CH_3CN): 1840.1 (9%) $[\{FeLZn(\mu\text{-}BNPP)\}_2(\mu\text{-}O)(ClO_4)]^+$; 871.1 (100%) $[\{FeLZn(\mu\text{-}BNPP)\}_2(\mu\text{-}O)]^{2+}$. Anal. Calcd for $C_{72}H_{68}Cl_2Fe_2N_{12}O_{29}P_2Zn_2$: C, 44.56; H, 3.53; N, 8.66. Found: C, 44.82; H, 3.59; N, 8.60. FT-IR (KBr, ν/cm^{-1}): 3435(br), 1637(s), 1600(w), 1560(m), 1558(m), 1489(w), 1410(w), 1346(s), 1213(m), 1090(s,br), 912(m), 856(m), 816(w), 762(m), 625(m), 523(w). UV−vis [CH_3CN, λ_{max}/nm (ϵ/M^{-1} cm^{-1})]: 365 (21 500). Λ_M (CH_3CN/Ω^{-1} cm^2 M^{-1}): 265.

Physical Measurements. Elemental (C, H, and N) analyses were performed on a Perkin-Elmer 2400II elemental analyzer. IR spectra were recorded using KBr disks on a Shimadzu FTIR 8400S spectrometer. The electronic absorption spectra were obtained with a Perkin-Elmer 950 UV/vis/NIR spectrophotometer. The electrospray ionization mass spectra (ESI-MS) were measured on a Micromass Qtof YA 263 mass spectrometer. The ^{1}H NMR (300 MHz) spectra were recorded on a Bruker Avance DPX-300 spectrometer. Longitudinal relaxation times (T_1) were measured by the inversion−recovery method. The T_1 values were obtained by the fitting of magnetization recovery curves that were exponential in nature. The transverse relaxation times (T_2) were estimated from the peak half-widths. Magnetic susceptibility measurements were carried out on a SQUID magnetometer (MPMS Quantum Design) over the temperature range 2−300 K. The magnetic field applied was 1.0 T. Diamagnetic corrections were made by using Pascal's

---

(35) Perrin, D. D.; Dempsey, B. *Buffers for pH and Metal Ion Control*; Chapman and Hall: London, 1974.

(36) (a) Ullman, F.; Brittner, K. *Chem. Ber.* **1909**, *42*, 2539. (b) Gagne, R. R.; Spiro, C. L.; Smith, T. J.; Hamman, C. A.; Theis, W. R.; Shiemke, A. K. *J. Am. Chem. Soc.* **1981**, *103*, 4073.

(37) Dutta, B.; Bag, P.; Adhikary, B.; Flörke, U.; Nag, K. *J. Org. Chem.* **2004**, *69*, 5419.

(38) Dutta, B.; Adhikary, B.; Bag, P.; Flörke, U.; Nag, K. *J. Chem. Soc., Dalton Trans.* **2002**, 2760.

(39) Moffatt, J. G.; Khorana, H. G. *J. Am. Chem. Soc.* **1957**, *79*, 3741.

Table 1. Crystallographic Data for **4** and **6**

	4	**6**
empirical formula	$C_{52}H_{60}Cl_2Fe_2N_8O_{18}Zn_2$	$C_{72}H_{68}Cl_2Fe_2N_{12}O_{29}P_2Zn_2$
fw	1398.42	1940.66
T, K	123(2)	120(2)
crystal syst, space group	monoclinic, $P2_1/c$	monoclinic, $P2_1/c$
a, Å	10.3190(7)	14.2859(5)
b, Å	18.3198(14)	19.2184(7)
c, Å	14.6518(11)	14.7702(5)
α, deg	90	90
β, deg	94.828(2)	96.001(1)
γ, deg	90	90
V, Å^3	2760.0(3)	4033.0(2)
Z, ρ_{calcd}, Mg m^{-3}	2, 1.683	2, 1.598
μ, mm^{-1}	1.553	1.137
$F(000)$	1984	1436
cryst size, mm^3	0.30 × 0.25 × 0.22	0.40 × 0.28 × 0.19
no. of data/restraints/params	6941/51/416	9618/28/546
no. of reflns [$I > 2\sigma(I)$]	34811	40312
GOF on F^2	0.999	0.967
final R indices [$I > 2\sigma(I)$]	R1^a = 0.0527, wR2^b = 0.1115	R1^a = 0.0513, wR2^b = 0.1248
R indices (all data)	R1^a = 0.0794, wR2^b = 0.1212	R1^a = 0.0732, wR2^b = 0.1339

^{a} $R1(F) = \Sigma||F_o| - |F_c||/\Sigma|F_o|$. ^{b} $wR2(F^2) = [\Sigma w(F_o^2 - F_c^2)^2/\Sigma w(F_o^2)^2]^{1/2}$.

constant. Molar conductivities (Λ_M) for a 1 mM solution of complexes **1**−**6** in acetonitrile were measured at 25 °C with a Systronics conductivity bridge. The electrochemical measurements of complexes **1**−**4** in acetonitrile were performed at 25 °C under a nitrogen atmosphere using a Bioanalytical Systems BAS 100B electrochemical analyzer. The concentration of the supporting electrolyte tetrabutylammonium perchlorate was 0.1 M, while that of the complex was 1 mM. Cyclic voltammetric (CV) and square-wave voltammetric (SWV) measurements were carried out with a three-electrode assembly comprising either a platinum or glassy carbon disk working electrode, a platinum auxiliary electrode, and an aqueous Ag/AgCl reference electrode. IR compensation was made automatically during each run. Under the experimental conditions used, the $E_{1/2}$ value of the ferrocene/ferrocenium couple was 440 mV.

The equilibrium constant for the aquation of $[Fe(LH_2)(H_2O)Cl]^{2+}$ (**1**$^{2+}$) to $[Fe(LH_2)(H_2O)_2]^{3+}$ (**2**$^{3+}$) was determined by spectrophotometric titration at 25 °C of **1**$^{2+}$ in acetonitrile with incremental addition of water. The equilibrium constant for the dimerization of **2**$^{3+}$ to $[\{Fe(LH_2)(H_2O)\}_2(\mu\text{-}O)]^{4+}$ (**3**$^{4+}$) was also determined by recording absorption spectra at 25 °C for a series of acetonitrile−water (1:1) solutions of **2**$^{3+}$ containing the same amount of the complex species and adding buffer solutions in the pH range 5−12, while keeping the acetonitrile−water ratio 1:1 and the total volume of the solution fixed. Spectrophotometric titrations were also carried out for complexes **1**−**3** in acetonitrile with tetramethylammonium chloride to determine the equilibrium constants involving binding of the chloride ion to the metal center(s). The kinetics of the formation of $[\{ZnLFe(\mu\text{-}OAc)\}_2(\mu\text{-}O)]^{2+}$ (**4**$^{2+}$) from **1**$^{2+}$ and **3**$^{2+}$ by reacting them with an excess of $Zn(OAc)_2\cdot 2H_2O$ at 25 °C in 1:1 acetonitrile−water at pH 6.6 were followed spectrophotometrically.

Crystal Structure Determinations of 3, 4, and 6. Crystals suitable for structure determinations of **3**, **4**, and **6** were obtained by slow evaporation of their acetonitrile−ethanol solutions. The crystals were mounted on glass fibers using perfluoropolyether oil. Intensity data were collected on a Bruker-AXS SMART APEX diffractometer at 123(2) K using graphite-monochromated Mo Kα radiation (λ = 0.710 73 Å). The data were processed with *SAINT*,[40] and absorption corrections were made with *SADABS*.[40] The structures were solved by direct and Fourier methods and refined by full-matrix least-squares methods based on F^2 using *SHELX-97*.[41] For the structure solutions and refinements, the *SHELX-TL* software package[42] was used. The non-hydrogen atoms were refined anisotropically, while the hydrogen atoms were placed at geometrically calculated positions with fixed thermal parameters.

The structure of complex **3** [$C_{48}H_{64}Cl_4Fe_2N_8O_{25}$, M = 1406.6, monoclinic, space group $P2_1/n$, a = 15.377(4) Å, b = 16.425(4) Å, c = 23.278(7) Å, α = 90°, β = 108.877(6)°, γ = 90°, U = 5563(3) Å^3, Z = 4, D = 1.440 g cm^{-3}] could not be refined satisfactorily because of severe disordering problems related to some of the carbon atoms of the macrocycles as well as the perchlorate anions and the water molecules. Nevertheless, essential structural information of the compound was obtained.

The crystallographic data for **4** and **6** are given in Table 1. In the case of **4**, the carbon atom C1 is disordered over two positions, C101 and C102, and these were refined with occupations of 0.60(2) and 0.40(2), respectively. The perchlorate anion was also disordered over two positions with a half-occupation each with common O11, O12, and O13 positions. The oxygen atom of the solvent water has an occupation factor of 0.5.

In the case of compound **6**, the nitro group N6O9O10 is disordered over two sites with an occupation factor of 0.5 each. Consequently, the aromatic ring C31−C36 also shows disorder (large anisotropic behavior for some of the carbon atoms) but could not be modeled. The same is true for the perchlorate ion, showing large U_{ij} for the oxygen atoms.

Results and Discussion

Syntheses. The syntheses of complexes **1**−**6** are outlined in Scheme 1. The mononuclear iron(III) complex **1** is obtained by the metathetical reaction between $[Pb(LH_2)](ClO)_2$ and $FeCl_3\cdot 6H_2O$, while the diaqua complex **2** is prepared by reacting $Fe(ClO_4)_3\cdot 6H_2O$ with the perchlorate salt of the macrocycle $[H_2LH_2](ClO_4)_2$. In these compounds, LH_2 represents the zwitterionic state of the macrocycle where

---

(40) *SAINT*, version 6.02; *SADABS*, version 2.03; Bruker AXS lnc.: Madison, WI, 2002.

(41) Sheldrick, G. M. *SHELXL-97, Program for the Refinement of Crystal Structures*; University of Göttingen, Göttingen, Germany, 1997.

(42) *SHELXTL*, version 6.10; Bruker AXS Inc.: Madison, WI, 2002.

Scheme 1

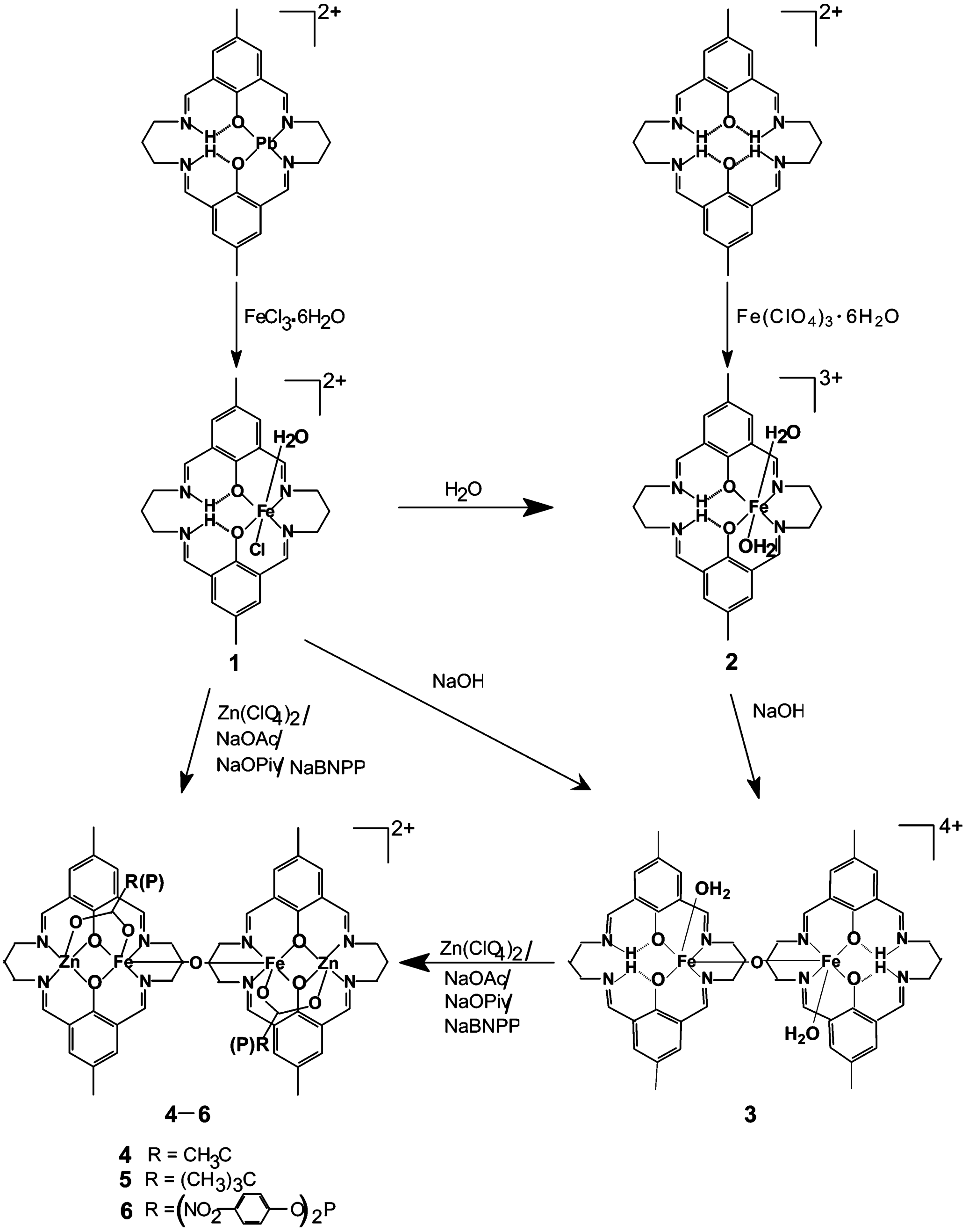

the two phenolic protons are transferred to two of the uncoordinated imine nitrogens. Both compounds **1** and **2** upon treatment with 1 equiv of aqueous alkali undergo dimerization to produce the oxo-bridged compound **3**. When compound **1** is reacted with 1 equiv of $Zn(ClO_4)_2·6H_2O$ and an excess of sodium acetate, sodium pivalate, or BNPP, the corresponding carboxylate- or phosphate-bridged heterobimetallic compounds **4**−**6** are obtained. Compounds **4**−**6** can also be prepared directly from **3** by reacting it with 2 equiv of $Zn(ClO_4)_2·6H_2O$ and the sodium salts of the bridging anions.

Characterization. Compounds **3**−**6** have been characterized by ESI-MS positive measurements in acetonitrile. As expected for **3** [Figure S1(a) in the Supporting Information], the ionic species $[Fe_2(LH_2)_2(\mu\text{-}O)(ClO_4)_3]^+$ (m/z = 1234.9), $[Fe_2(LH_2)(LH)(\mu\text{-}O)(ClO_4)_2]^+$ (m/z = 1134.5), and $[Fe_2(LH)_2(\mu\text{-}O)(ClO_4)]^+$ (m/z =1034.1) have been detected, albeit as weak peaks. In the case of **4** [Figure S1(b) in the Supporting Information], although the peak due to $[\{FeLZn(\mu\text{-}OAc)\}_2(\mu\text{-}O)(ClO_4)]^+$ (m/z = 1280.6) is relatively weak (6%), the dication $[\{FeLZn(\mu\text{-}OAc)\}_2(\mu\text{-}O)]^+$ (m/z = 590.2) appears as the base peak (100%). A similar observation has been made for **6**, whose observed and simulated spectral patterns for the cations $[\{FeLZn(\mu\text{-}BNPP)\}_2(\mu\text{-}O)(ClO_4)]^+$ (9%) and $[\{FeLZn(\mu\text{-}BNPP)\}_2(\mu\text{-}O)]^{2+}$ (100%) are shown in Figure 1.

The IR spectra of the complexes exhibit several diagnostic features. A weak band observed between 3160 and 3170 cm^{-1} in **1**−**3** is due to the N−H stretching vibration of the protonated imine, which is hydrogen-bonded to the phenolate

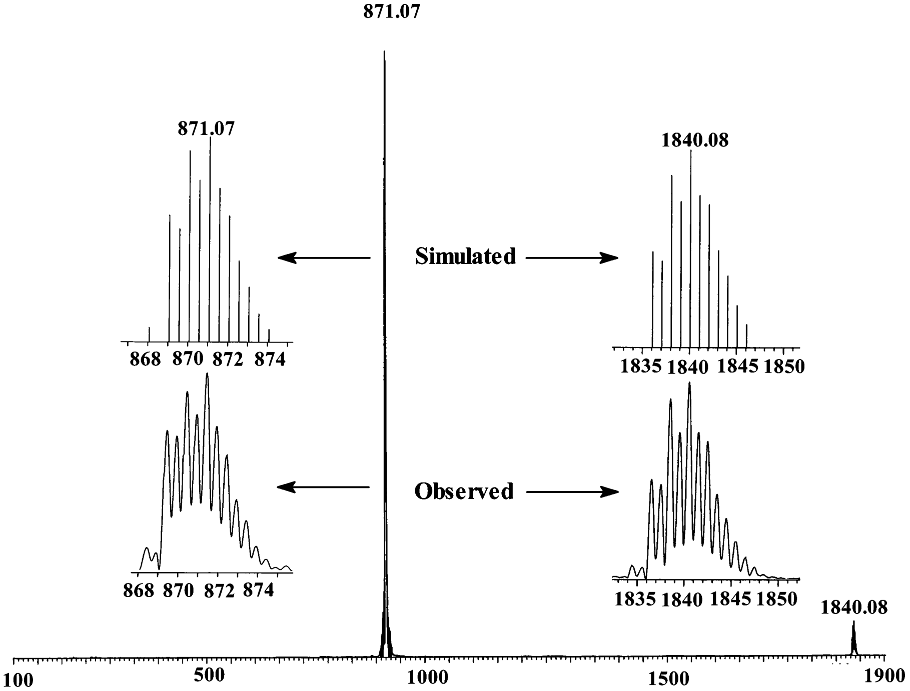

Figure 1. Isotopic distribution of the observed and simulated ESI-MS (positive) of **6** in acetonitrile.

oxygen. The metal-coordinated and metal-free C=N vibrations in these three compounds are observed as two separate bands in the vicinities of 1660 and 1625 cm^{-1}. However, in the heterobimetallic complexes **4**−**6**, the $\nu_{C=N}$ bands due to the two metal centers are shifted to about 1635 and 1605 cm^{-1}. For the carboxylate-bridged complexes **4** and **5**, the ν_{as} CO_2^- and ν_s CO_2^- bands are observed at about 1564 and 1508 cm^{-1}, respectively, and their separation by 156 cm^{-1} is consistent with the bridging mode of binding.[43] Compounds **3**−**6** having a Fe−O−Fe linkage exhibit a band of medium intensity due to the ν_{as} Fe−O−Fe vibration in the range of 847−856 cm^{-1}. As will be seen, in these compounds the Fe−O−Fe angle is 180° for **4** and **6** and 169° for **3**. For a number of oxo-bridged diiron(III) compounds, a correlation between the energy of the ν_{as} Fe−O−Fe vibration and the angle involved in it has been reported.[44]

The electrical conductivities for complexes **1**−**6** have been measured in acetonitrile (1×10^{-3} M). The molar conductivity (Λ_M) of **1** in acetonitrile (290 Ω^{-1} cm^2 M^{-1}) is consistent with the values expected for 1:2 electrolytes (220−300 Ω^{-1} cm^2 M^{-1} in acetonitrile),[45] indicating that the chloride ion remains bound to the metal center. For the other complexes (1:3 for **2**, 1:4 for **3**, and 1:2 for **4**−**6**), the expected electrolytic behavior has also been observed.

The UV−vis spectra of all of the complexes have been obtained in acetonitrile. **1** exhibits three absorption bands at 385 nm (ϵ = 13 800 M^{-1} cm^{-1}), 435 nm (sh), and 530 nm (ϵ = 3600 M^{-1} cm^{-1}), while for **2**, only two peaks are observed at 375 nm (13 500 M^{-1} cm^{-1}) and 555 nm (3200 M^{-1} cm^{-1}). On the other hand, both of the compounds exhibit identical spectra in 1:1 acetonitrile−water with the peaks at 365 nm (13 100 M^{-1} cm^{-1}) and 530 nm (3600 M^{-1} cm^{-1}). It appears that although iron(III) prefers the aqua ligand, this preference is not enough to resist the replacement of the aqua ligand(s) by acetonitrile in **1** and **2** upon their dissolution in this solvent. Despite the 1:2 electrolytic nature of **1** in acetonitrile, the identical spectra observed for **1** and **2** in 1:1 acetonitrile−water suggest that in this solvent medium the Fe−Cl bond in **1** undergoes ionic dissociation and the observed spectrum is due to the species $[Fe(LH_2)(H_2O)_2]^{3+}$. The oxo-bridged diiron(III) complex **3** in 1:1 acetonitrile−water exhibits an asymmetric spectrum with a peak at 390 nm (28 000 M^{-1} cm^{-1}), an ill-defined shoulder at about 440 nm, and a broad envelope at around 515 nm (3900 M^{-1} cm^{-1}). On the other hand, in acetonitrile, although the peak position of **3** remains practically unaffected at 392 nm (29 000 M^{-1} cm^{-1}), the shoulder is blue-shifted to 425 nm and the higher-wavelength absorption band merges to the part of continuous absorption. Clearly, in **3** the aqua ligand gets substituted by the solvent molecule. The oxo-bridged diiron(III) complexes are known to exhibit several symmetry-related oxo → iron(III) charge-transfer transitions whose energies depend on the Fe−O−Fe bridge angle.[46,47] When this angle is close to linearity, a band is observed between 300 and 500 nm due to an oxo → iron(III) d_{xz} and d_{yz} transition of π symmetry. As the Fe−O−Fe angle deviates from linearity, this band gets split. For the oxo-bridged iron(III)−zinc(II) complexes **4**−**6**, the lone absorption band at 360−365 nm (21 000−25 000 M^{-1} cm^{-1}) is

---

(43) Nakamoto, K. *Infrared and Raman Spectra of Inorganic and Coordination Compounds*, 5th ed.; VCH-Wiley: New York, 1997.

(44) Sanders-Loehr, J.; Wheeler, W. D.; Shiemke, A. K.; Averill, B. A.; Loehr, T. M. *J. Am. Chem. Soc.* **1989**, *111*, 8084.

(45) Geary, W. J. *Coord. Chem. Rev.* **1971**, *7*, 81.

(46) Brown, C. A.; Remar, G. J.; Musselman, R. L.; Solomon, E. I. *Inorg. Chem.* **1995**, *34*, 688.

(47) Schugar, H. J.; Rossman, G. R.; Barraclough, C. G.; Gray, H. B. *J. Am. Chem. Soc.* **1972**, *94*, 2689.

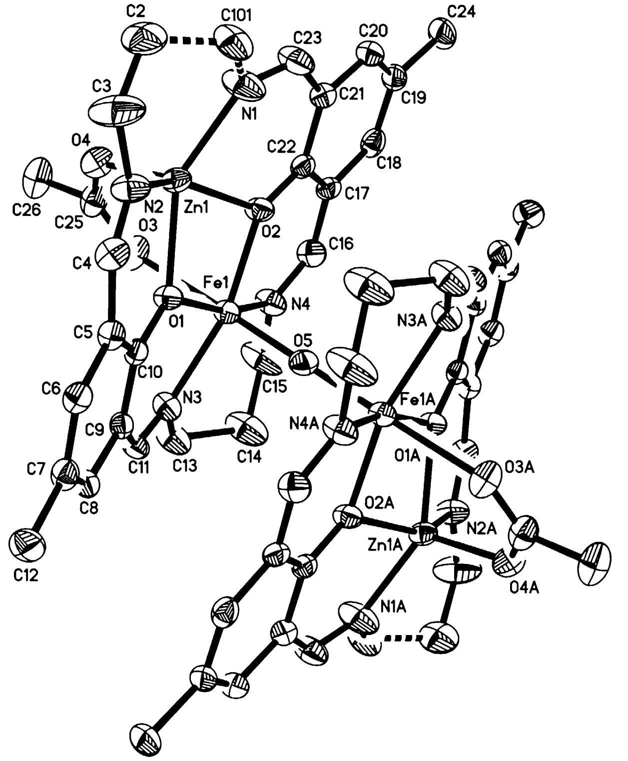

Figure 2. ORTEP representation of the cation $[\{FeLZn(\mu\text{-}OAc)\}_2(\mu\text{-}O)]^{2+}$ in **4** showing 50% probability displacement ellipsoids.

due to a μ-O$_\pi$ → iron(III) charge-transfer transition. The reaction equilibria involving the exchange of terminal ligands ($H_2O/CH_3CN/Cl^-$) in complexes **1**−**3** have been studied separately by spectrophotometric and electrochemical methods (see later).

Crystal Structures. As was already mentioned, because of severe disordering, the structure of **3** could not be refined satisfactorily. Nevertheless, in this compound the iron(III) center is six-coordinated with a N_2O_2 basal plane and a water molecule is trans-axially disposed to the Fe−O−Fe linkage. The average Fe−O(oxo) distance is 1.76(3) Å, and the Fe−O−Fe angle is 168.6(2)°.

The structure of the cation $[\{FeLZn(\mu\text{-}OAc)\}_2(\mu\text{-}O)]^{2+}$ in **4**, as shown in Figure 2, is comprised of two heterobimetallic macrocyclic units. The μ-O5 atom lies on a crystallographic inversion center, and therefore the Fe−O−Fe bridge is exactly linear. In the asymmetric unit, the iron(III) and zinc(II) centers are triply bridged by the two phenoxides of the macrocycle and an acetate ligand. Each of the metal centers is additionally coordinated by two imine nitrogens of the macrocycle. The iron(III) center thus obtains a distorted octahedral geometry, while the coordination environment around zinc(II) is distorted square-pyramidal. The carbon atom C1 of the propylene lateral chain is disordered over two sites, C101 and C102, with site occupations of 0.60(2) and 0.40(2), respectively; the major position is shown in Figure 2. The perchlorate anion is also disordered over two sites with equal (0.5) occupancy and has common O11, O12, and O13 positions. Selected bond distances and bond angles are given in Table 2.

Table 2. Selected Bond Distances (Å) and Angles (deg) for **4** and **6**

4		6	
Fe−O1	1.991(2)	Fe−O1	2.002(2)
Fe−O2	1.995(2)	Fe−O2	2.024(2)
Fe−O3	2.221(3)	Fe−O4	2.185(2)
Fe−O5	1.7744(5)	Fe−O11	1.7807(4)
Fe−N3	2.084(3)	Fe−N3	2.085(3)
Fe−N4	2.078(3)	Fe−N4	2.078(3)
Zn−O1	2.059(2)	Zn−O1	2.094(2)
Zn−O2	2.097(2)	Zn−O2	2.092(2)
Zn−O4	1.962(2)	Zn−O3	1.984(2)
Zn−N1	2.042(3)	Zn−N1	2.032(3)
Zn−N2	2.042(3)	Zn−N2	2.026(3)
Fe···Fe*	3.549(1)	Fe···Fe*	3.561(1)
Fe···Zn	3.101(1)	Fe···Zn	3.161(1)
O1−Fe−O2	80.80(9)	O1−Fe−O2	79.77(8)
O1−Fe−O3	83.39(10)	O1−Fe−O4	84.33(8)
O1−Fe−O5	97.52(7)	O1−Fe−O11	98.09(6)
O2−Fe−O3	82.34(10)	O2−Fe−O4	84.98(8)
O2−Fe−O5	98.75(7)	O2−Fe−O11	101.03(6)
O3−Fe−O5	178.67(7)	O4−Fe−O11	173.82(6)
O1−Fe−N3	88.79(10)	O1−Fe−N4	89.80(9)
O1−Fe−N4	165.67(11)	O1−Fe−N3	166.27(9)
O2−Fe−N3	165.22(11)	O2−Fe−N4	164.49(9)
O2−Fe−N4	90.57(11)	O2−Fe−N3	89.80(9)
O3−Fe−N3	86.09(11)	O4−Fe−N4	82.57(9)
O3−Fe−N4	84.15(11)	O4−Fe−N3	85.88(9)
O5−Fe−N3	92.95(11)	O11−Fe−N4	91.73(7)
O5−Fe−N4	95.07(9)	O11−Fe−N3	92.63(7)
N3−Fe−N4	97.38(12)	N3−Fe−N4	98.47(10)
O1−Zn−O2	76.84(9)	O1−Zn−O2	76.15(8)
O1−Zn−O4	94.25(10)	O1−Zn−O3	92.89(9)
O2−Zn−O4	95.49(10)	O2−Zn−O3	97.98(9)
O1−Zn−N1	148.13(14)	O1−Zn−N2	157.62(10)
O1−Zn−N2	87.11(11)	O1−Zn−N1	85.96(9)
O2−Zn−N1	85.17(12)	O2−Zn−N2	88.33(9)
O2−Zn−N2	148.71(12)	O2−Zn−N1	142.58(9)
O4−Zn−N1	113.69(14)	O3−Zn−N1	115.74(10)
O4−Zn−N2	112.55(12)	O3−Zn−N2	105.33(10)
N1−Zn−N2	95.41(13)	N1−Zn−N2	97.34(11)
Fe−O5−Fe*	180.0(0)	Fe−O11−Fe*	180.0(0)
Fe−O1−Zn	99.90(10)	Fe−O1−Zn	100.97(9)
Fe−O2−Zn	98.51(10)	Fe−O2−Zn	100.31(9)

The donor atoms O1, O2, N1, and N2 around zinc(II) form an exact plane from which the metal atom is displaced toward the apical coordination site O4 of the bridging acetate by 0.533(3) Å. The average Zn−O(phenolate), Zn−N(imine), and Zn−O(acetate) distances are 2.078(18), 2.042(1), and 1.962(2) Å, respectively. In the basal plane, two of the opposing angles, O1−Zn−O2 [76.84 (9)°] and N1−Zn−N2 [95.41 (13)°], differ considerably, whereas the other two opposing angles, N1−Zn−O2 [85.17(12)°] and N2−Zn−O1 [87.11 (11)°], are nearly equal. Again, the transverse angles N1−Zn−O1 and N2−Zn−O2 are identical [148.13(14)° and 148.71(12)°].

The iron(III) atom is displaced from the least-squares basal plane of O1, O2, N3, and N4 toward the oxo ligand O5 by 0.211(2)°. The two Fe−O(phenolate) distances [1.991(2) and 1.995(2) Å] are identical, as are the two Fe−N(imine) distances [2.078(3) and 2.084 (3) Å]. On the other hand, the axial Fe−O(acetate) distance [2.221(3) Å] is significantly longer relative to the Fe−O(oxo) distance [1.7744(5) Å]. Aside from the Fe−O−Fe angle being 180.0°, the trans-axial O3−Fe−O5 angle is also nearly linear [178.67(7)°]. In the asymmetric unit, the two heterometal atoms are separated by 3.1006(7) Å with the intervening Fe−O−Zn

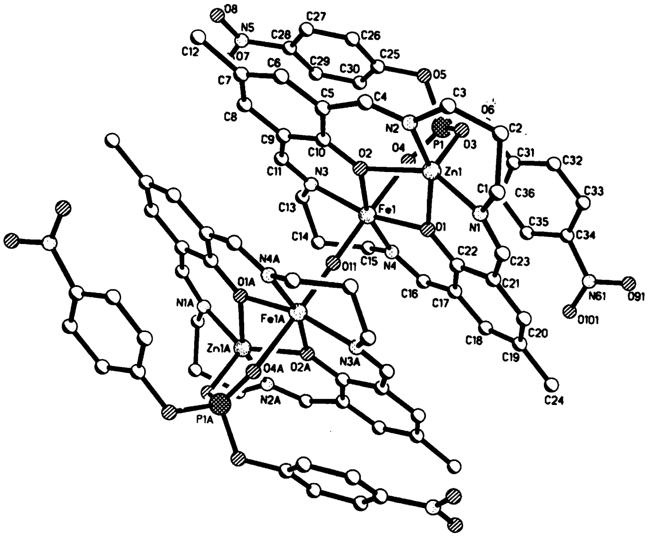

Figure 3. Structural projection for the cation $[\{\mathrm{FeLZn}(\mu\text{-BNPP})\}_2(\mu\text{-O})]^{2+}$ in **6**.

bridge angles 99.90(10)° and 98.5(10)°. The dihedral angle between the basal planes of the two metals is 8.3°, while the planes of the aromatic rings make an angle of 16.1°.

A structural projection for the cation $[\{\mathrm{FeLZn}(\mu\text{-BNPP})\}_2(\mu\text{-O})]^{2+}$ in **6** is shown in Figure 3. Similar to **4**, in this case also the oxygen atom O11 connecting the two heterobimetallic $\mathrm{Zn^{II}Fe^{III}}$ units by the Fe−O−Fe linkage lies on a crystallographic inversion center. Again, the zinc(II) and iron(III) centers are five- and six-coordinated, respectively. As was already mentioned, the para-nitro group [N6O9O10] is disordered over two sites with equal occupancy. Selected bond distances of **6** are compared with those of **4** in Table 2. It may be noted that the metrical parameters of the two compounds are closely similar. The $\mathrm{PO_4}$ moiety of BNPP in **6** is roughly tetrahedral, with the O−P−O angles varying between 96.7° and 118.7° [average 108(11)°]. The two metal-bound P−O distances [P−O3 = 1.493(2) Å and P−O4 = 1.487(2) Å] are relatively shorter with respect to the aromatic-ring-bound P−O distances [P−O5 = 1.594(2) Å and P−O6 = 1.605(2) Å]. Moreover, as compared to the Fe−O(phenolate) distances [Fe−O1 = 2.002(2) Å and Fe−O2 = 2.024(2) Å], the Fe−O(phosphate) distance [Fe−O4 = 2.185(2) Å] is considerably longer. In contrast, the Zn−O(phenolate) distances [Zn−O1 = 2.094(2) Å and Zn−O2 = 2.092(2) Å] are longer relative to the Zn−O(phosphate) distance [Zn−O3 = 1.984(2) Å]. Although the separation between the iron centers in the Fe−O−Fe units of **4** [3.549(1) Å] and **6** [3.561(1) Å] are practically same, the intramolecular Fe···Zn distances in **4** [3.101(1) Å] and **6** [3.161(1) Å] are somewhat different.

Reaction Equilibria and Kinetics. As was already mentioned, in acetonitrile, the aqua ligands $\mathbf{1}^{2+}$ and $\mathbf{2}^{3+}$ undergo exchange with solvent molecules and the solvated species revert back to the diaqua complex $[\mathrm{Fe(LH_2)(H_2O)_2}]^{3+}$ in an acetonitrile−water medium. The aquation/solvation reaction equilibria (1) have been studied spectrophotometrically, and the equilibrium constant K_{aq} for the aquation of $\mathbf{1}^{2+}$ to $\mathbf{2}^{3+}$ has been determined.

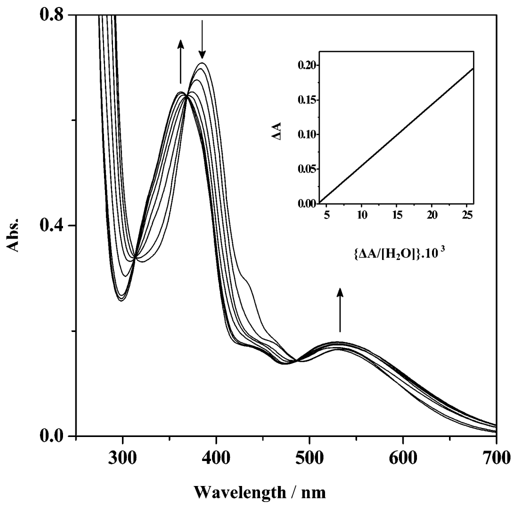

Figure 4. Spectrophotometric titration of **1** in acetonitrile with water. The inset shows the plot for the evaluation of K_{aq} according to eq 2.

$$\begin{tikzcd}[\mathrm{Fe(LH_2)(H_2O)Cl}]^{2+} \arrow[r, shift left, "K_{aq}"] \arrow[d, shift left, "\mathrm{CH_3CN}"] & {[\mathrm{Fe(LH_2)(H_2O)_2}]^{3+} + \mathrm{Cl^-}} \arrow[l, shift left] \arrow[d, shift left, "\mathrm{CH_3CN}"] \\ {[\mathrm{Fe(LH_2)(CH_3CN)Cl}]^{2+}} \arrow[u, shift left, "\mathrm{H_2O}"] & {[\mathrm{Fe(LH_2)(CH_3CN)_2}]^{3+}} \arrow[u, shift left, "\mathrm{H_2O}"]\end{tikzcd} \tag{1}$$

Figure 4 shows the spectral changes that occur when an acetonitrile solution of **1** is titrated with water. It may be noted that with the incremental addition of water the peak observed at 385 nm is blue-shifted to 365 nm with diminution of the intensity, while the broad peak at 540 nm is intensified to a small extent. The successive absorption curves pass through the isosbestic points at 314, 369, and 486 nm.

The equilibrium constant K_{aq} has been evaluated using the relations[48] (2) and (3). In these expressions, ΔA_{max} is the

$$\Delta A = \Delta A_{max} - K_{aq}(\Delta A/[\mathrm{H_2O}]) \tag{2}$$

$$[\mathrm{H_2O}] = C_{\mathrm{H_2O}} - C_1(\Delta A/\Delta A_{max}) \tag{3}$$

maximum change in absorption obtainable with the addition of water, ΔA is the change of absorption near the maximum at a given point of titration, $C_{\mathrm{H_2O}}$ is the concentration of water added, and C_1 is the concentration of complex **1**. The inset of Figure 4 shows a linear plot of ΔA vs $\Delta A/[\mathrm{H_2O}]$, the slope of which gives $K_{aq} = 8.75(5)\ \mathrm{M^{-1}}$.

Inasmuch as the electrical conductivity of **1** in acetonitrile indicates that the chloride remains bonded to the metal center in $[\mathrm{Fe(LH_2)(CH_3CN)Cl}]^{2+}$, it has been of interest to see whether a second chloride ion could be coordinated to the metal center. Accordingly, an acetonitrile solution of **1** has been spectrophotometrically titrated with tetramethylammonium chloride. Figure 5 shows that smooth spectral changes occur through three isosbestic points at 320, 390, and 503 nm, and the final spectrum has the following features: λ_{max}

---

(48) Brown, K. L. *Inorg. Chim. Acta* **1979**, *37,* L513.

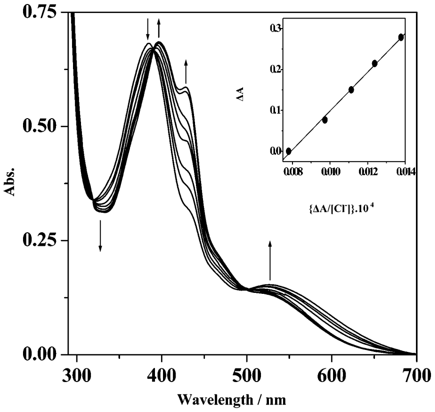

Figure 5. Spectrophotometric titration of **1** in acetonitrile with various equivalents of tetramethylammonium chloride added. The inset shows the plot for the evaluation of K_{Cl^-}.

$= 397$ nm ($\epsilon = 13\,800$ M^{-1} cm^{-1}), 428 nm (11 800 M^{-1} cm^{-1}), and 530 nm (3100 M^{-1} cm^{-1}). The equalibrium constant K_{Cl^-} for the dichloro complex formation (eq 4) is 4.75(5) M^{-1}.

$$\begin{tikzcd}[\mathrm{Fe(LH_2)(H_2O)Cl}]^{2+} \arrow[rr, shift left, "\mathrm{CH_3CN}"] \arrow[dr, shift left, "\mathrm{Cl^-}"'] & & {[\mathrm{Fe(LH_2)(H_2O)_2}]^{3+}} \arrow[ll, shift left, "\mathrm{H_2O}"] \arrow[dl, shift left, "\mathrm{Cl^-}"'] \\ & {[\mathrm{Fe(LH_2)Cl_2}]^{+}} \arrow[ul, shift left] \arrow[ur, shift left] & \end{tikzcd} \tag{4}$$

As expected, the interactions of cholride ions with the diaqua complex **2** occur in two steps. The spectral changes (Figure S2 in the Supporting Information) are accompanied by the formation of the monochloro and dichloro complex species (eq 5).

$$[\mathrm{Fe(LH_2)(H_2O)_2}]^{3+} \underset{\mathrm{H_2O}}{\overset{\mathrm{CH_3CN}}{\rightleftharpoons}} [\mathrm{Fe(LH_2)(CH_3CN)_2}]^{3+} \overset{\mathrm{Cl^-}}{\rightleftharpoons} [\mathrm{Fe(LH_2)(CH_3CN)Cl}]^{2+} \overset{\mathrm{Cl^-}}{\rightleftharpoons} [\mathrm{Fe(LH_2)Cl_2}]^{+} \tag{5}$$

In an aqueous acetonitrile solution, the diaqua complex cation $\mathbf{2}^{3+}$ undergoes a dimerization reaction to the oxo-bridged diiron(III) species $\mathbf{3}^{4+}$ with an increase of the pH. The dimerization constant K_D for the reaction equilibrium equation (6) has been determined spectrophotometrically.

$$\mathbf{2}^{3+} \overset{K_D}{\rightleftharpoons} \mathbf{3}^{4+} + 2\mathrm{H}^+ + \mathrm{H_2O} \tag{6}$$

Figure 6 shows the spectral changes that occur when a solution of **2** in 1:1 acetonitrile−water is progressively treated with a sodium hydroxide solution in the same solvent. The successive absorption curves pass through the isosbestic points at 325, 370, and 485 nm, and with the addition of a stoichiometric amount of hydroxide, the final spectrum becomes identical with that of $\mathbf{3}^{4+}$ in 1:1 acetonitrile−water, that is, with $\lambda_{max} = 390$ nm (28 000 M^{-1} cm^{-1}), 440(sh), and 515 nm (3900 M^{-1} cm^{-1}). The value of K_D has been evaluated using eq 7.[49] In this expression, A_2 and A_3 are the

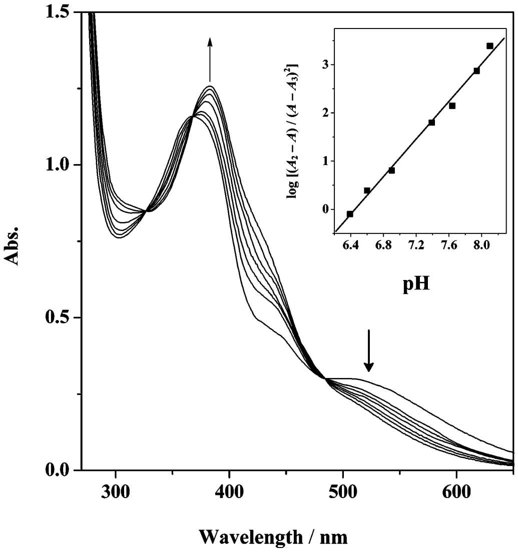

Figure 6. Spectrophotometric titration of **2** in 1:1 acetonitrile−water with sodium hydroxide. The inset shows the plot for the evaluation of K_D according to eq 5.

$$\log[(A_2 - A)/(A - A_3)^2] = \log K_D - 2 \log [\mathrm{H}^+] + \log[4/(\epsilon_2 - \epsilon_3)] \tag{7}$$

absorbances of the monomer **2** and dimer **3**, while A is the absorbance of the equilibrium mixture at a given wavelength. Similarly, ϵ_2 and ϵ_3 refer to the molar absorptivities of **2** and **3**, respectively. The inset of Figure 6 shows that a plot of $\log[(A_2 - A)/(A - A_3)^2]$ vs pH at $\lambda = 350$ nm gives a straight line with a slope equal to 2.01. The average value of $\log K_D$ obtained from the intercepts of similar plots at 350, 420, and 440 nm is 9.38(10).

Similar to complexes **1** and **2**, the aqua ligand of **3** also undergoes exchange with solvent acetonitrile. More importantly, chloride binding occurs to the metal centers in **3** in the same way (as shown in Figure S3 in the Supporting Information). The reaction equilibrium equation (8) is completely shifted to the right-hand side when a 10-fold excess of tetramethylammonium chloride is added. The

$$[\{\mathrm{Fe(LH_2)(H_2O)}\}_2(\mu\text{-O})]^{4+} \underset{\mathrm{H_2O}}{\overset{\mathrm{CH_3CN}}{\rightleftharpoons}} [\{\mathrm{Fe(LH_2)(CH_3CN)}\}_2(\mu\text{-O})]^{4+} \overset{\mathrm{Cl^-}}{\rightleftharpoons} [\{\mathrm{Fe(LH_2)Cl}\}_2(\mu\text{-O})]^{2+} \tag{8}$$

formation of the heterobimetallic complex $\mathbf{4}^{2+}$ has been followed spectrophotometrically after equilibriating a series of solutions containing equimolar mixture **1** and $\mathrm{Zn(ClO_4)_2 \cdot 6H_2O}$ and with increasing equivalents of sodium acetate in 1:1 acetonitrile−water. Figure 7 shows that while the absorption curves pass through the isosbestic points at 312 and 368 nm, the more intense peak at 386 nm gradually

---

(49) Fleischer, E. B.; Palmer, J. M.; Srivastava, T. S.; Chatterjee, A. *J. Am. Chem. Soc.* **1971**, *93*, 3162.

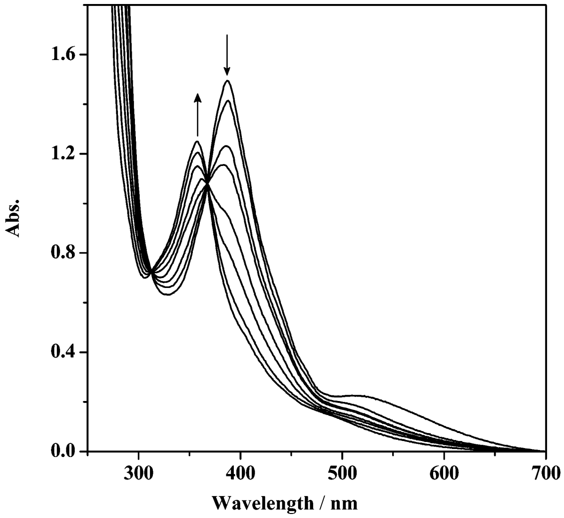

Figure 7. Spectrophotometric titration of a 1:1 mixture of **1** and $Zn(ClO4)_2{\cdot}6H_2O$ in 1:1 acetonitrile−water with sodium acetate showing the formation of $[\{FeLZn(\mu\text{-}OAc)\}_2(\mu\text{-}O)]^{2+}$.

disappears at the expense of evolution of a less intense peak at 360 nm. After 6 equiv of sodium acetate was added, the spectrum becomes identical with that of $\mathbf{4}^{2+}$. The reaction stoichiometry (eq 9) indicates that the role of excess acetate is to provide a buffer effect and to shift the reaction to the right-hand side. It appears that the overall reaction (9) takes place in a stepwise manner. Two possibilities may be considered. The first is to consider the sequential reactions in eqs 10 and 11. The second possibility is that $[Fe(LH_2)(H_2O)Cl]^{2+}$ dimerizes first to $[\{Fe(LH_2)(H_2O)\}_2(\mu\text{-}O)]^{4+}$ in the presence of sodium acetate, which then reacts with Zn^{2+} and OAc^- to form heterobimetallic complex $\mathbf{4}^{2+}$ (eq 12).

$$[Fe(LH_2)(H_2O)Cl]^{2+} + 2Zn^{2+} + 2OAc^- \rightarrow [\{FeLZn(\mu\text{-}OAc)\}_2(\mu\text{-}O)]^{2+} + 6H^+ + H_2O + 2Cl^- \quad (9)$$

$$[Fe(LH_2)(H_2O)Cl]^{2+} + Zn^{2+} + OAc^-(\text{excess}) \rightarrow [(H_2O)FeLZn(OAc)]^{2+} + 2H^+ + Cl^- \quad (10)$$

$$2[(H_2O)FeLZn(OAc)]^{2+} \rightarrow [\{FeLZn(\mu\text{-}OAc)\}_2(\mu\text{-}O)]^{2+} + 2H^+ + H_2O \quad (11)$$

$$[\{Fe(LH_2)(H_2O)\}_2(\mu\text{-}O)]^{4+} + 2Zn^{2+} + 2OAc^-(\text{excess}) \rightarrow [\{FeLZn(\mu\text{-}OAc)\}_2(\mu\text{-}O)]^{2+} + 4H^+ + 2H_2O \quad (12)$$

To understand the reaction mechanism involved in the formation of $\mathbf{4}^{2+}$, kinetic studies have been made for the reactions involving **1** or **3** and a 10-fold excess of $Zn(OAc)_2{\cdot}2H_2O$ in acetonitrile−water (1:1) at pH 6.6 and 25 °C. In both the cases, under the same experimental conditions, the observed rate constant K_{obs} for the formation of $\mathbf{4}^{2+}$ turns out to be the same as $1.6(2) \times 10^{-4}\ s^{-1}$.

This indicates that the rate-determining step for the formation of the product must be identical for both cases and, hence, must be controlled by the rate of insertion of zinc(II) into $[\{Fe(LH_2)(H_2O)\}_2(\mu\text{-}O)]^{4+}$ according to eq 13.

$$[\{Fe(LH_2)(H_2O)\}_2(\mu\text{-}O)]^{4+} + 2Zn(OAc)_2 \rightarrow [\{FeLZn(\mu\text{-}OAc)\}_2(\mu\text{-}O)]^{2+} + 2OAc^- + 4H^+ + 2H_2O \quad (13)$$

Under the experimental conditions used, the concentration of $Zn(OAc)_2$ is high (10-fold excess), and therefore the concentration of acetate also remains high. Moreover, the hydrogen ion concentration also remains fixed (pH 6.6). Accordingly, eq 14 simplifies to a first-order reaction because the rate of formation of $\mathbf{4}^{2+}$ is dependent only upon the concentration of $\mathbf{3}^{4+}$. The first-order plot is shown in the inset of the cover page.

$$\text{rate} = k_{obs}\frac{[\{FeLZn(\mu\text{-}OAc)\}_4(\mu\text{-}O)][OAc^-]^2[H^+]^4}{[\{Fe(LH_2)(H_2O)\}_2(\mu\text{-}O)^{4+}][Zn(OAc)_2]^2} = k_{obs}\frac{[\mathbf{4}^{2+}][OAc^-]^2[H^+]^2}{[\mathbf{3}^{4+}][Zn(OAc)_2]^2} \quad (14)$$

Electrochemistry. The electrochemical behavior of complexes **1**−**4** has been studied in acetonitrile. In view of the lability of the terminal ligands in complexes **1**−**3**, electrochemical measurements are complementary to the spectrophotometric studies.

The cyclic voltammogram of complex **1** in acetonitrile (shown in the lowermost part of Figure 8a) exhibits the presence of two poorly resolved redox couples. The square-wave voltammogram of this compound upon deconvolution (shown in Figure S4 in the Supporting Information) gives two peaks with $E_{1/2} = 200$ and 80 mV. Clearly, because complex **1** in acetonitrile is an equilibrium mixture of the species $[Fe(LH_2)(CH_3CN)Cl]^{2+}$ and $[Fe(LH_2)(H_2O)Cl]^{2+}$, they undergo reductions at two different potentials. When this solution is treated with a small amount of water (acetonitrile−water, 10:0.1), the two redox couples converged into one with $E_{1/2} = 140$ mV. Figure 8a shows that with a decrease of the acetonitrile−water ratio, $E_{1/2}$ remains unchanged, but the quasi-reversible redox couple changes to a fully reversible one ($\Delta E_p = 70$ mV) when the solvent ratio is 10:1. As will be seen, at this stage, the observed CV feature is identical with that of $\mathbf{2}^{3+}$. The progressive change of the electrochemical behavior of **1** with a variation of the solvent composition is consistent with the reaction equilibria given in eq 1.

A dramatic change of the redox behavior takes place when the acetonitrile solution of **1** is treated with an increasing amount of tetramethylammonium chloride (as shown Figure 8b). It may be noted that the broad overlapping quasi-reversible redox features with the $E_{1/2}$ value(s) at positive potential(s) change to a single redox couple with increased reversibility. Further, the $E_{1/2}$ values decrease progressively as the equivalents of chloride added is increased. Finally, beyond 8 equiv of chloride added, no further change occurs, and the resulting $[Fe(LH_2)Cl_2]^+$ species has $E_{1/2} = -80$ mV

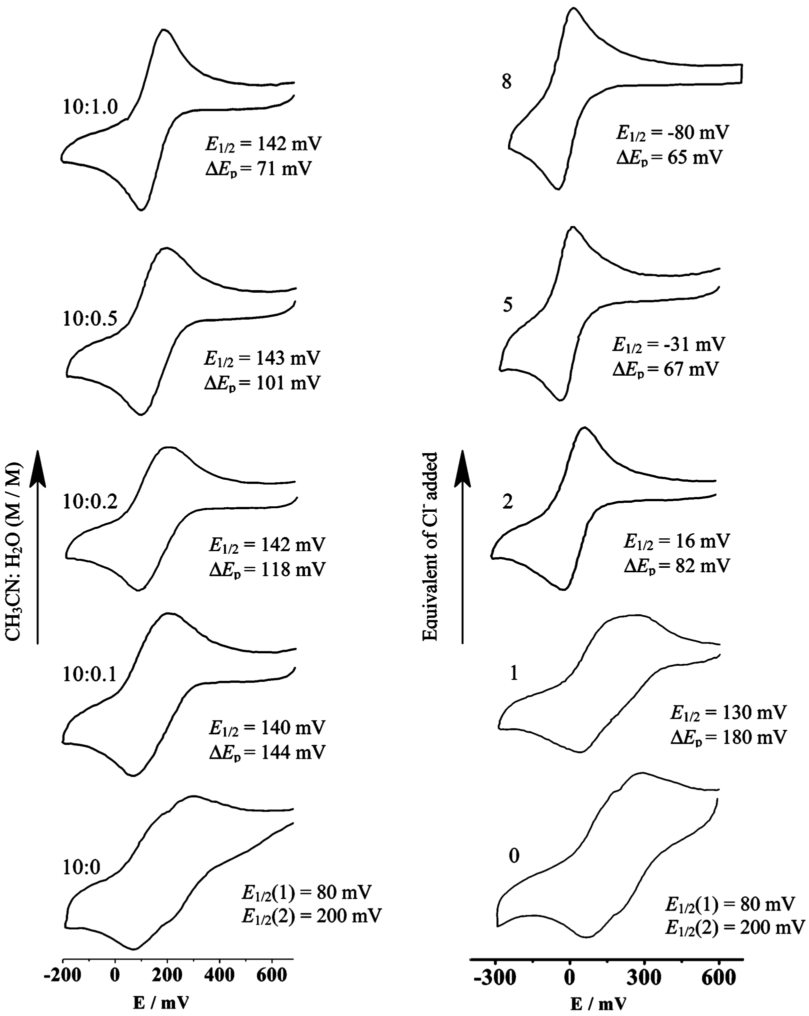

(a) (b)

Figure 8. Cyclic voltammograms of **1** in acetonitrile−water with the indicated ratios of acetonitrile−water (a) and in acetonitrile with the indicated equivalents of Cl^- (tetramethylammonium chloride) added (b). The scan rate in all cases was 100 mV s^{-1}.

and $\Delta E_p = 65$ mV. The change of the redox pattern is again consistent with the reaction equilibria given by eq 4. It is easy to see that with the addition of the chloride ion the cationic charge of complex **1** is decreased, and therefore the addition of an electron to the resulting dichloro complex becomes more difficult.

The exchange of aqua ligands in $\mathbf{2}^{3+}$ by acetonitrile and vice versa and the interaction of the solvated species with the chloride ion have been studied electrochemically. As shown in Figure 9a, the cyclic voltammogram of complex **2** in acetonitrile exhibits an almost reversible couple ($\Delta E_p = 80$ mV) with $E_{1/2} = 358$ mV. When a small amount of water is added to the solution (acetonitrile−water, 10:0.1), the single redox couple splits into two, with their $E_{1/2}$ values 365 and 240 mV, indicating that, in addition to the earlier species, a new species coexists in solution. A further increase of the water proportion leads to the disappearance of the original species, and eventually when the solvent ratio becomes 10:0.7, a clean reversible cyclic voltammogram ($\Delta E_p = 70$ mV) with $E_{1/2} = 142$ mV is obtained. It is important to note that this voltammogram is identical with the one obtained for complex **1** in 10:1 acetonitrile−water (topmost cyclic voltammogram of Figure 8a). Thus, the observed changes in the electrochemical behavior of complex **2** with a variation of the acetonitrile−water ratio are indicative of the occurrence of the stepwise exchange reactions in eq 15.

$$[Fe(LH_2)(CH_3CN)_2]^{3+} \underset{CH_3CN}{\overset{H_2O}{\rightleftharpoons}} [Fe(LH_2)(CH_3CN)(H_2O)]^{3+} \underset{CH_3CN}{\overset{H_2O}{\rightleftharpoons}} [Fe(LH_2)(H_2O)_2]^{3+} \quad (15)$$

In Figure 9b, the effect of adding various (1−10) equivalents of tetramethylammonium chloride to the acetonitrile solution of **2** is shown. As may be noted, the $E_{1/2}$ value undergoes a shift by about 440 mV as $[Fe(LH_2)(CH_3CN)_2]^{3+}$ ($E_{1/2} = 358$ mV) changes via $[Fe(LH_2)(CH_3CN)Cl]^{2+}$ to $[Fe(LH_2)Cl_2]^+$ ($E_{1/2} = -80$ mV).

The redox property of the oxo-bridged diiron(III) complex $\mathbf{3}^{4+}$ has been considered to be of interest because the exchange of a terminal aqua ligand with acetonitrile and substitution by chloride would have a profound effect on the redox potential, especially on stabilization of the unusual $Fe^{III}-O-Fe^{II}$ unit. Two recent studies have reported spectroscopic and electrochemical characterization of aqua ligand-

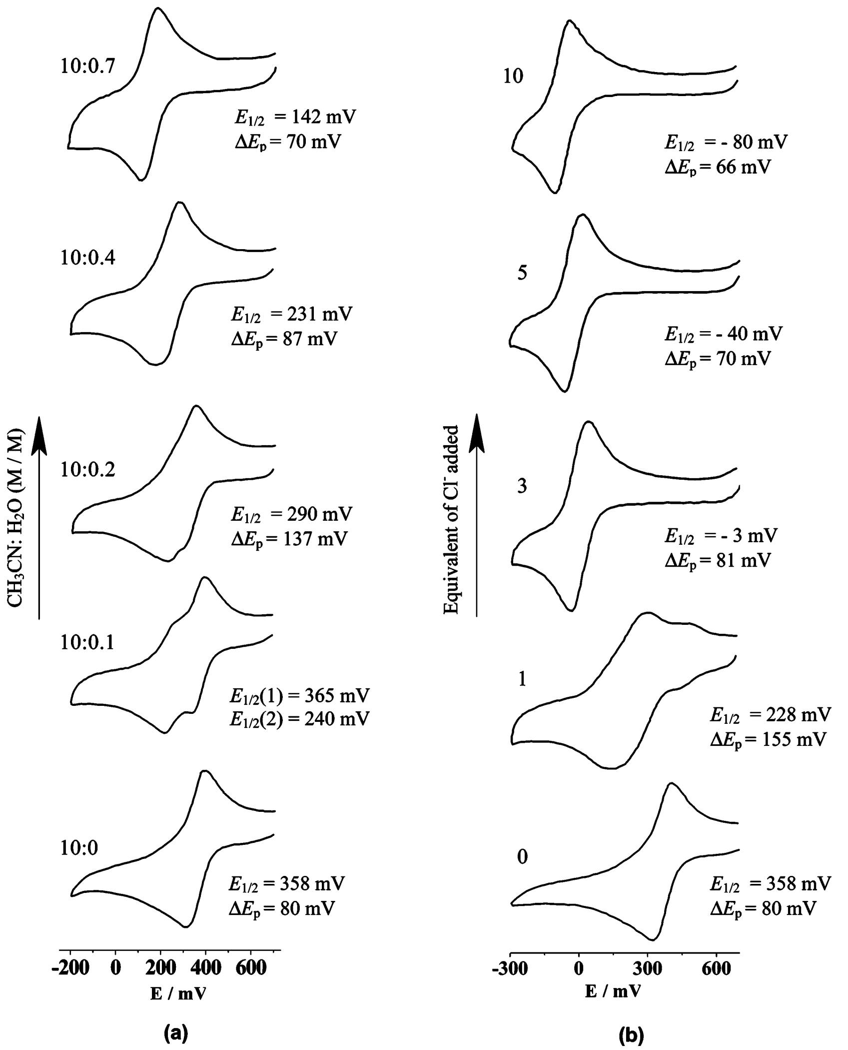

Figure 9. Cyclic voltammograms of **2** in acetonitrile−water with the indicated ratios of acetonitrile−water (a) and in acetonitrile with the indicated equivalents of Cl^- (tetramethylammonium chloride) added (b). The scan rate in all cases was 100 mV s^{-1}.

exchanged diiron complexes[50] and electrochemically generated $Fe^{III}{-}O{-}Fe^{II}$ species.[51]

As shown in Figure 10a, complex **3** in acetonitrile in the potential range of +600 to −400 mV exhibits two cathodic responses at +130 and −100 mV, while in the return anodic sweep, a plateau at ca. +30 mV and a peak at +260 mV are observed. When the scan range is limited to +600 to 0 mV, a quasi-reversible voltammogram with $E_{1/2} = 195$ mV and $\Delta E_p = 130$ mV is obtained. The electron-transfer process involved in this particular reaction is given by eq 16. Further

$$[(CH_3CN)(LH_2)Fe^{III}{-}O{-}Fe^{III}(LH_2)(CH_3CN)]^{4+} \overset{e^-}{\rightleftharpoons} [(CH_3CN)(LH_2)Fe^{III}{-}O{-}Fe^{II}(LH_2)(CH_3CN)]^{3+} \quad (16)$$

electron transfer occurring at $E_{p,c} = -100$ mV leads to decomposition in a complicated way owing to the inherent instability of $Fe^{II}{-}O{-}Fe^{II}$.

When the above acetonitrile solution of $\mathbf{3}^{4+}$ is treated with an increasing amount of tetramethylammonium chloride, the cyclic voltammogram recorded in the potential range of +600 to −400 mV exhibits a single redox couple with a varying $E_{1/2}$ value (see Figure 9a). The variation of the $E_{1/2}$ value with the equivalents of chloride added is shown in Figure 10b. It may be noted that the redox potential monotonically decreases from +195 mV with the addition of chloride and finally the $E_{1/2}$ value levels off at −120 mV when about 10 equiv of chloride is added. This observation is consistent with the previously described spectrophotometric titration. Referring back to eq 8, the chloride-assisted electron-transfer reaction is given by eq 17.

$$[(CH_3CN)(LH_2)Fe^{III}{-}O{-}Fe^{III}(LH_2)(CH_3CN)]^{4+} \overset{Cl^-}{\rightleftharpoons} [Cl(LH_2)Fe^{III}{-}O{-}Fe^{III}(LH_2)Cl]^{2+} \overset{e^-}{\rightleftharpoons} [Cl(LH_2)Fe^{III}{-}O{-}Fe^{II}(LH_2)Cl]^{+} \quad (17)$$

The cyclic voltammogram of the iron(III)−zinc(II) complex $\mathbf{4}^{2+}$ in acetonitrile recorded over the potential range of +500 to −1200 mV (Figure 11) shows two cathodic peaks of $E_{p,c}$ at −380 and ca. −700 mV and two anodic peaks *of*

---

(50) Chardon-Noblat, S.; Horner, O.; Avenier, F.; Debaecker, N.; Jones, P.; Pecaut, J.; Dubois, L.; Jeandey, C.; Latour, J.-M. *Inorg. Chem.* **2004**, *43*, 1638.

(51) Nivorozhkin, A. L.; Anoxlabehere-Mallat, E.; Milane, M.; Audiere, J. P.; Girerd, J.-J.; Styring, S.; Schussler, L.; Seri, J.-L. *Inorg. Chem.* **1997**, *36*, 846.

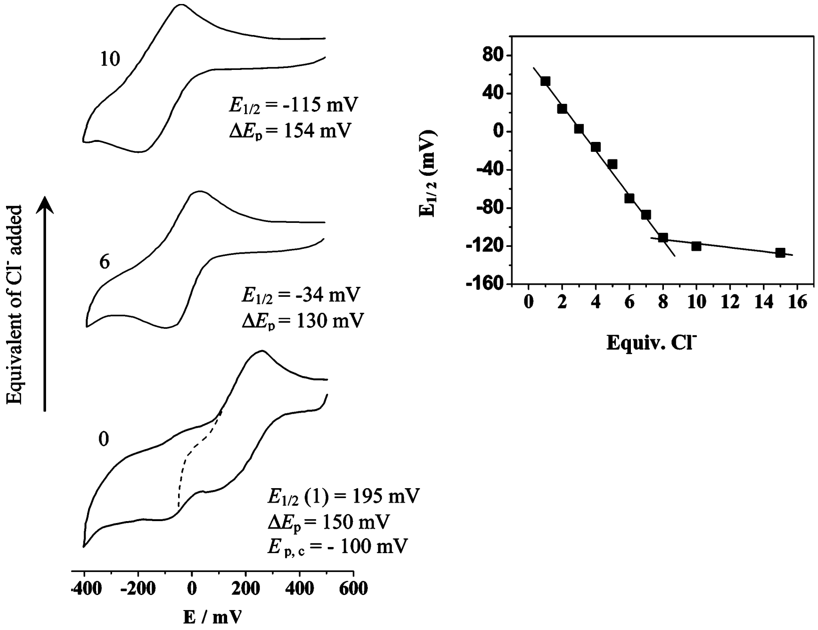

Figure 10. Cyclic voltammograms of **3** in acetonitrile along with the changes observed for the first redox couple with the addition of 5 and 8 equiv of tetramethylammonium chloride. The scan rate was 100 mV s^{-1}. The inset shows the plot of $E_{1/2}$ (for the first redox couple) vs equivalents of chloride added.

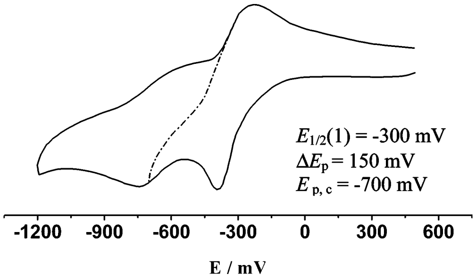

Figure 11. Cyclic voltammograms of **4** in acetonitrile at a scan rate of 100 mV s^{-1}.

$E_{p,a}$ at −220 and ca. −550 mV. When the scan range is kept between 500 and −600 mV, a quasi-reversible voltammogram with $E_{1/2} = -300$ mV and $\Delta E_p = 150$ mV is obtained. As may be seen in Figure 11, the other two peaks are broad and ill-defined and therefore indicate that the electron-transfer reactions are associated with chemical reactions. The observation of the quasi-reversible redox couple

$$[Zn^{II}L(\mu\text{-OAc})Fe^{III}{-}O{-}Fe^{III}(\mu\text{-OAc})LZn^{II}]^{2+}/$$
$$[Zn^{II}L(\mu\text{-OAc})Fe^{III}{-}O{-}Fe^{II}(\mu\text{-OAc})LZn^{II}]^{+}$$

indicates that oxo-bridged mixed-valence iron is stable at least in the CV time scale (as verified by variation of the scan rate between 500 and 50 mV s^{-1}).

Redox properties of oxo-bridged diiron(III) complexes derived from polydentate ligands in combination with auxiliary bridging ligands have been the subject of several studies.[51−53] The addition of the first electron resulting from the formation of the mixed-valent species in most of these cases has been reported to occur reversibly or quasi-reversibly, and the redox potential spans over positive to negative values. The second-electron addition occurs almost invariably in an irreversible manner. We are not aware of any oxo-bridged $Fe^{II}Fe^{III}$ complex isolated in the solid state, which probably is due to the strong tendency of the $Fe^{III}{-}O{-}Fe^{II}$ unit to undergo disproportionation in solution.[52,53]

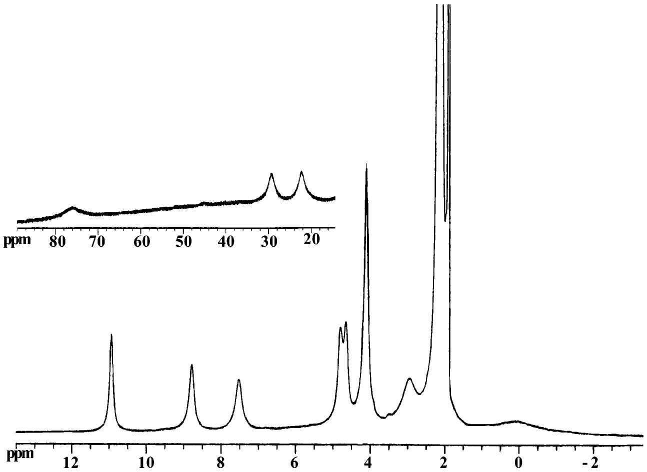

Figure 12. ^1H NMR spectrum of **4** in CD_3CN.

^{1}H NMR Spectra. The ^1H NMR spectra of complexes **3**−**6** have been measured in CD_3CN and $(CD_3)_2SO$. The peak positions of the compounds remain almost unchanged in the two solvents. The spectrum of **4** is shown in Figure 12, while those of **3**, **5**, and **6** are available as Supporting Information (Figure S5). Because the heterobimetallic complexes **4**−**6** as well as **3** have C_2 symmetry, a total number of nine signals (designated as a−h in Table 3) for the macrocyclic ring protons are expected. As may be noted in the spectra of complexes **4**−**6**, the bridging carboxylate or phosphate ligands get dissociated from the metal centers and they are observed in their normal diamagnetic positions. Thus, OAc^- of **4** is observed at 2.47 ppm (Figure 12), $OPiv^-$ of **5** is

---

(52) Hartman, J. R.; Rardin, R. L.; Chaudhuri, P.; Pohl, K.; Wieghardt, K.; Nuber, R.; Weiss, J.; Papaefthymiou, G. C.; Frankel, R. B.; Lippard, S. J. *J. Am. Chem. Soc.* **1987**, *109*, 7387.

(53) Holz, R. C.; Elgren, T. E.; Pearce, L. L.; Zhang, J. H.; O'Connor, C. J.; Que, L., Jr. *Inorg. Chem.* **1993**, *32*, 5844.

Table 3. Chemical Shifts, T_1 Values, Line Widths, Fe···H Distances, and Spectral Assignments for **4** in CD_3CN

				Fe···H/Å		
δ/ppm	relative area	T_1/ms	$\Delta_{1/2}$/Hz[a]	X-ray	solution	assignment[b]
77	4	<1	2400	3.7		CH_2(f)
29.4	2	0.9	850	3.8	4.4	=CH(d)
22.4	2	1	800	4.0	4.5	CH_2(g)
10.95	2	7.9	250	6.2	6.4	Ar(c)
8.79	2	5.3	270	5.8	6.0	=CH(e)
7.54	2	2.7	400	5.2	5.4	Ar(b)
4.80	4	8.6	100	6.5	6.5	CH_2(h)
4.66	2	8.5	120	6.7	6.6	CH_2(i)
4.16	6	18.4[c]	60	7.4[c]		CH_3(a)
2.47[d]	3		20			OAc

[a] Full width at half-height. [b] Proton sites are illustrated below. [c] Reference values. [d] Acetate dissociated from the metal centers.

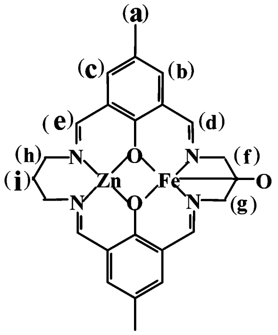

Table 4. Hyperfine-Shifted Signals and Their Assignments[a] for **3**, **5**, and **6** in CD_3CN

3			**5**			**6**		
δ/ppm	rel. area	assign.	δ/ppm	rel. area	assign.	δ/ppm	rel. area	assign.
90	4	CH_2(f)	77	4	CH_2(f)	76	4	CH_2(f)
44	2	=CH(d)	27.4	2	=CH(d)	36	2	=CH(d)
18.3	2	CH_2(g)	24.4	2	CH_2(g)	17	2	CH_2(g)
12.07	2	=CH(e)	10.94	2	Ar(c)	10.69	2	Ar(c)
9.23	4	Ar(b,c)	8.71	2	=CH(e)	8.61	2	=CH(e)
5.60	4	CH_2(h)	7.49	2	Ar(b)	7.20	2	Ar(b)
5.41	6	CH_3(a)	4.67	6	CH_2(h,i)	4.78	4	CH_2(h)
3.0	2	CH_2(i)	3.96	6	CH_3(a)	4.52	2	CH_2(i)
			0.98[b]	9	OPiv	4.04	6	CH_3(**a**)
						7.72[c]	4	$BNPP^-$
						6.88[c]	4	$BNPP^-$

[a] Illustration of the proton sites is the same as that in Table 3. [b] Metal-free pivalate anion. [c] Metal-free BNPP anion.

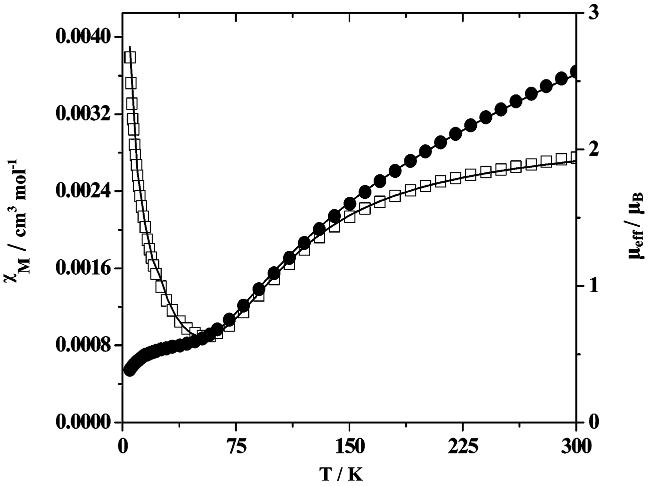

Figure 13. Molar magnetic susceptibility (□) and effective magnetic moment (●) per iron(III) vs temperature for **4**. The solid lines result from a least-squares fit to the theoretical expression given in ref 55.

observed at 0.99 ppm [Figure S5(b) in the Supporting Information], and the aromatic protons due to $BNPP^-$ of **6** are observed at 6.68 and 7.72 ppm [Figure S5(c) in the Supporting Information]. The room-temperature magnetic moments of compounds **3**−**6** are quiet low, ca. 2.4 μ_B/Fe^{III}, because of a strong antiferromagnetic exchange interaction between the high-spin iron(III) centers in the Fe−O−Fe unit. Accordingly, the hyperfine-shifted signals for all of the compounds are observed in the range 0−90 ppm, of which most of the signals, barring three, are quite sharp.

Signal assignment for **4**, which is typical of the $Fe^{III}Zn^{II}$ compounds, has been accomplished by measuring relaxation times T_1 and T_2 and taking into consideration the number of protons associated with each signal. Proton longitudinal relaxation time T_1 correlates the proximity of the proton to the paramagnetic site, as does transverse relaxation time T_2, which is $1/\pi\Delta_{1/2}$, where $\Delta_{1/2}$ is the full width of a signal at half-height. Thus, for closer proximity of a proton to the paramagnetic metal center, a shorter T_1 and a broader line width are to be expected.[54] The results of these measurements for **4**, based on which signal assignments have been made, are given in Table 3. Because T_1 has a r^6 dependence on the metal−proton distances ($r_{Fe\cdots H}$), using relative T_1 values corresponding $r_{Fe\cdots H}$ distances have been obtained for **4** by the relation $r_{Fe\cdots H} = r_{ref}(T_1/T_{ref})^{1/6}$, where r_{ref} and T_{ref} are the reference values.

The Fe···H distances for **4** in the solid state and in solution are compared in Table 3. Fairly good agreements between these values indicate correctness of the signal assignments. The assignments of the hyperfine-shifted signals of the structurally related compounds **5** and **6** as well as **3** have been made straightforwardly in comparison with **4** and are listed in Table 4. In the case of **3**, the hydrogen-bonded imino protons could not be detected because of extensive line broadening.

Magnetic Properties. Variable-temperature magnetic susceptibility measurements have been carried out for **3** and **4** between 2 and 300 K. The plots of χ_M and μ_{eff} vs T per iron(III) for **3** and **4** are shown in Figure S6 in the Supporting Information and Figure 13, respectively. For both of the compounds, the magnetic moments decrease, from about 2.5 μ_B at 300 K, with a decrease of the temperature and reach a plateau of ca. 0.3 μ_B at about 60 K, which is consistent for strongly antiferromagnetically coupled $S = {}^5/_2$ pairs. The nonzero value of μ_{eff} for the plateau between 60 and 10 K indicates the presence of a small amount of mononuclear impurity. The χ_M vs T data have been subjected to a least-squares fit to the expression[55] derived from the spin Hamiltonian $H = -2JS_1 \cdot S_2$, where $S_1 = S_2 = {}^5/_2$.

---

(54) (a) Bertini, I.; Turano, P.; Vila, A. *Chem. Rev.* **1993**, *93*, 2883. (b) Bertini, I.; Luchinat, C. *NMR of Paramagnetic Substances*; Elsevier: Amsterdam, The Netherlands, 1996.

The best-fit parameters thus obtained are

3:

$$J = -114\ \mathrm{cm}^{-1},\ g = 1.98,\ p = 0.8\%,\ \mathrm{TIP} = 200 \times 10^{-6}\ \mathrm{cm}^3\ \mathrm{mol}^{-1},\ \text{and}\ R = 2.80 \times 10^{-3}$$

4:

$$J = -107\ \mathrm{cm}^{-1},\ g = 1.98,\ p = 0.8\%,\ \mathrm{TIP} = 200 \times 10^{-6}\ \mathrm{cm}^3\ \mathrm{mol}^{-1},\ \text{and}\ R = 2.86 \times 10^{-3}$$

The dependence of J on the Fe−O−Fe angle φ and the average Fe−O distance (r) has been analyzed by an angular and radial overlap model[56] and is given by eq 18.

$$-2J_{\mathrm{model}} = 1.337 \times 10^{8}(3.536 + 2.488 \cos \varphi + \cos^2 \varphi) \exp(-7.909r) \quad (18)$$

For complex **4** with $\varphi = 180°$ and $r = 1.7744$ Å, the calculated value of $J = -110\ \mathrm{cm}^{-1}$ is in excellent agreement with the experimental value $-107\ \mathrm{cm}^{-1}$. In the case of **3**, for which the structural parameters ($\varphi = 168.6°$ and $r = 1.76$ Å) are less accurate because of disordering, the difference between the calculated J value ($-124\ \mathrm{cm}^{-1}$) and the experimentally observed value ($-114\ \mathrm{cm}^{-1}$) is more.

Conclusion

The chemistry of the mononuclear iron(III) complexes **1** and **2**, the oxo-bridged diiron complex **3**, and the oxo-bridged heterobimetallic iron(III)−zinc(II) complexes **4**−**6** with bridging carboxylate moieties has been studied. In complexes **1**−**3**, the terminal ligands H_2O/Cl^- undergo solvation (in acetonitrile) and aquation (in acetonitrile−water). They also interact with the chloride ion in acetonitrile. The reaction equilibria involved in these cases have been studied by a combination of spectrophotometric and electrochemical methods. The Fe−H_2O linkage in **1** or **2** undergoes dimerization when treated with alkali in an aqueous acetonitrile to produce the oxo-bridged species $\mathbf{3}^{4+}$. Complexes **1**−**3** upon reaction with either zinc(II) perchlorate and an excess of sodium acetate or zinc(II) acetate produce the heterobimetallic complex **4**. Kinetic studies have established that the formation of $\mathbf{4}^{2+}$ is preceded by fast generation of $\mathbf{3}^{4+}$. CV measurements of **1**−**3** have revealed that the $E_{1/2}$ values and the extent of reversibility of the systems are strongly dependent upon the solvent composition, that is, the acetonitrile−water ratio (from 10:0 to 10:1), as are the cases with a variation of the equivalents of chloride added. The observation of quasi-reversible cyclic voltammograms for the first reduction step of **3** and **4** in acetonitrile indicates that the unusual $\mathrm{Fe^{III}{-}O{-}Fe^{II}}$ unit is stable in a voltammetric time scale. The X-ray structure determinations have shown that although in **4** and **6** the Fe−O−Fe angle is perfectly linear, it is somewhat bent (168.6°) in **3**. Complexes **3**−**6** have been further characterized by their paramagnetic ^{1}H NMR spectra. The metal−hydrogen distances of **4** as obtained from T_1 measurements are in good agreement with those obtained from the X-ray structure determination. The high-spin iron(III) centers ($S = {}^5/_2$) in the oxo-bridged compounds are strongly antiferromagnetically coupled ($H = -2JS_1 \cdot S_2$) with $J = -114\ \mathrm{cm}^{-1}$ for **3** and $-107\ \mathrm{cm}^{-1}$ for **4**.

The ease with which the aquated iron(III) complex dimerizes to the oxo-bridged diiron(III) species points to the fact that for the design of a functional model for KBPAP the ligand assembly should ensure the prevention of dimerization of the iron(III) center. In KBPAP, hydrolysis of phosphate ester involves substrate binding to the zinc(II) site by replacement of the coordinated water, followed by nucleophilic attack by either the bridging hydroxide or the iron(III)-bound terminal hydroxide or water molecule. The present study shows that the major deterrant for the formation of either a terminal $\mathrm{Fe^{III}{-}OH}$ or the bridging $\mathrm{Fe^{III}{-}OH{-}Zn^{II}}$ is the dimerization reaction at the $\mathrm{Fe^{III}{-}H_2O}$ site leading to the formation of the oxo-bridged compound.

Acknowledgment. K.N. thanks Prof. K. Wieghardt for providing the SQUID magnetometer facility during his stay at Max-Planck Institute for Bioinorganic Chemistry at Mulheim, Germany. P.B. and M.G. are thankful to CSIR, India, for the award of a research fellowship.

Supporting Information Available: X-ray crystallographic files in CIF format for compounds **4** and **6** and Figures S1−S6. This material is available free of charge via the Internet at http://pubs.acs.org.

IC060183B

---

(55) O'Connor, C. J. *Prog. Inorg. Chem.* **1982**, *29*, 203. $\chi_M = (1 - p)(Ng^2\mu_B{}^2/kT)[\{2 \exp(2x) + 10 \exp(6x) + 28 \exp(12x) + 60 \exp(20x) + 110 \exp(30x)\}/\{1 + 3 \exp(2x) + 5 \exp(6x) + 7 \exp(12x) + 9 \exp(20x) + 11 \exp(30x)\}] + (4.375p/T) + \mathrm{TIP}$ and $R = [\sum(\chi_{\mathrm{obs}} - \chi_{\mathrm{calc}})^2/(\sum\chi_{\mathrm{obs}})^2]^{1/2}$, where $x = J/kT$, p is the mol % of mononuclear iron(III) impurity, TIP is the temperature-independent paramagnetism, and R is the agreement factor.

(56) Weihe, H.; Güdel, H. U. *J. Am. Chem. Soc.* **1997**, *119*, 6539.